

Reply to the interactive comment of referee#1 (Cecilio Quesada) on “Deciphering the metamorphic evolution of the Pulo do Lobo metasedimentary belt (SW Iberian Variscides)” by Irene Pérez-Cáceres et al. (Manuscript number se-2019-143).

We acknowledge the interactive comment made by Cecilio Quesada as referee. His suggestions have contributed to clarify some issues of the manuscript, which are now included in the revised version.

This review is focused on disputable interpretations of the regional geology rather than on the main topic of our manuscript. All of these regional issues are answered in the following paragraphs, though we have reorganized and grouped them in order to avoid unnecessary repetitions. The line numbers quoted correspond to the revised version of the manuscript with tracked changes (uploaded as supplementary file to this response).

1. Geological setting. A more inclusive geological setting has been made by adding sentences and new references to authors with interpretations complementary or alternative to ours (lines 110-111, 128-129, 140-142).

2. Division in units of the SPZ. Regarding nomenclature, we prefer to use the term “Pulo do Lobo” in a merely descriptive way. Thus, the term belt was used in the submitted version of our manuscript; nevertheless, and in order to avoid any confusion (as claimed by the reviewer), we have renamed now the two major units of the region as: “Pulo do Lobo domain” and “SPZ domain” (lines 160-162). The subdivision of these two major domains is as follows, according to geological mapping both in Spain and Portugal:

a) The Pulo do Lobo domain includes, from bottom to top, the following stratigraphic formations: i) the Pulo do Lobo Fm; ii) the Ribeira de Limas Fm; and iii) the Santa Iría Fm, which unconformably overlies the other two formations. The relatively minor mafic rocks are embedded in the Pulo do Lobo Fm.

b) The SPZ domain includes, from bottom to top: i) the Phyllite-Quartzite (PQ) Group; ii) the Volcano-Sedimentary Complex (CVS); and iii) the Culm or Flysch Group. The southern ZSP is dominated by the Flysch Group, except at the southernmost corner where underlying formations equivalent to the PQ and CVS crop out.

We realize that the Santa Iría Fm (Pulo do Lobo domain) and the Flysch Group of the SPZ might be considered as a single tectonosedimentary unit with younger ages southwards. However, in order to comprehensively describe the tectonostratigraphic evolution of each domain (particularly the Pulo do Lobo domain; section 2.1 of the manuscript), the division shown above seems preferable.

3. Age of the Santa Iría Fm. There are two sources of evidence for the age of the Santa Iría Fm. On the one hand, palynological data (Pereira et al., 2018) suggest a Late Famennian age. On the other hand, detrital zircon populations (Braid et al., 2011; Pérez-Cáceres et al., 2017) point to an early Carboniferous age. The latter age seems preferable due to the common palynomorph reworking shown in some papers (Lopes et al., 2014). Alternatively, partial rejuvenation of the zircon U/Pb system during low-grade metamorphism has been claimed to discard the sedimentary early Carboniferous age, though the detrital zircon populations are robust and highly concordant (particularly SHRIMP data). Anyway, the exact age of the Santa Iría Fm is neither definitely conclusive (see Pereira et al., 2018, comment and reply) nor crucial for the tectonic evolution of the region.

4. Incomplete sampling? The Pulo do Lobo, Ribeira de Limas and Santa Iría formations crop out from west to east (from Portugal to Spain) all along the Pulo do Lobo domain, without significant differences along strike. Hence, sampling latitude is irrelevant. We have sampled two transects which include the three formations of the Pulo do Lobo domain (they have been specified as requested; lines 234-239). Thus, we consider unfounded claiming that our sampling was incomplete. Furthermore, some of our samples (PLB-91 and 93) were collected from the same area where the presence of “lawsonite pseudomorphs” was quoted by Rubio Pascual et al. (2013). Concerning the “lousy precision” of our sampling sites (Fig. 1b), we already added UTM coordinates as supplementary information to the first version of the manuscript.

Regarding the metamafic rocks, our study was intentionally focused on the metapelites because they better recorded the successive episodes of deformation and, with the new techniques used, the PT conditions of the low-grade metamorphism can also be unveiled with relative accuracy. Future studies focused on the metabasites will be welcome, though keeping in mind that the age of these rocks is early Carboniferous (here again, zircon populations are robust and highly concordant, particularly SHRIMP data), which, in turn, precludes getting information on the early (Devonian) metamorphism of the Pulo do Lobo domain.

5. Sample preparation and interpretation of XRF data. The preparation of oriented aggregates of both whole-rock and <2 μm fractions strictly followed a well established international procedure to minimize detrital mica content. Obviously, direct discrimination at small grain sizes is a hard task. In our case, both sample fractions yielded similar results, thus suggesting (detrital) mica re-equilibration during M1 metamorphism. Concerning the mechanical rotation of pre-existing minerals, our textural observations and chemical data (Figs. 2 and 3) support the preservation of variably rotated M1 micas during D2, as already discussed in our first manuscript (section 5.1).

6. Lawsonite? The presence of lawsonite in the Pulo do Lobo domain is only based on the external rhomboidal shape of an aggregate of epidote crystals interpreted as a lawsonite pseudomorph (Rubio Pascual et al., 2013). However, lawsonite can be easily mistaken for other minerals, such as clinozoisite. Indeed, the phengites analyzed by these authors “were not particularly indicative of HP recrystallization”. Clearly, the lawsonite pseudomorph is an extremely weak evidence for HP metamorphism, which cannot defy our much more complete metamorphic study. Anyway, the claim for a first lawsonite-bearing mineral assemblage was already cited in our first manuscript (section 5.4).

7. Biotite? According to the peak temperatures obtained in our study, biotite could be present in the Pulo do Lobo Fm. Actually, Rubio Pascual et al. (2013) reported two chemical analyses corresponding to biotite. However, we did not identify biotite in any of our samples, possibly because this mineral is restricted to some –and scarce– particular lithologies. This issue has been included in the discussion (lines 567-570).

8. Sedimentary mélangé or tectonic mélangé? Our study (see also Pérez-Cáceres et al., 2015) suggests that the so-called Peramora mélangé is a sedimentary mélangé dominated by mafic olistholites, which were later affected by thrusting, thus resulting also in a tectonic mélangé (reference to Apalategui et al., 1983 has been deleted here, as requested; line 214). Despite the reviewer’s criticism, this twofold characterization of the Peramora outcrop has no contradiction. At other outcrops, the metamafic rocks seem to be intrusive in the Pulo do Lobo Fm. We realize, however, that the description of the Peramora rocks was a bit confusing and have rewritten it (lines 210-211).

9. Deformations recorded by the Santa Iría Fm. First of all, it is important to point out that we agree with the reviewer on two issues: i) three penetrative deformations affected the Pulo do Lobo and Ribeira de Limas Fms of the Pulo do Lobo domain; and ii) Santa Iría Fm unconformably overlies the Pulo do Lobo and Ribeira de Limas Fms. However, the reviewer believes that the Santa Iría Fm is only affected by the third deformation, while we state that it is affected by the last two of them (Fig. 2c). Regarding this issue, the reviewer’s argument seems a bit confusing, being apparently based on: i) “it exists a general agreement”(?) and ii) the ages of deformed and undeformed facies of the Gil Márquez pluton (we deal with the Gil Márquez pluton in the following point of our answer). By contrast, our statement that the Santa Iría Fm is affected by two of the three penetrative deformations in the Pulo do Lobo domain is supported by a detailed structural analysis, which includes: cleavage identification, deformational microstructures, local vergences and indicators of stratigraphic polarity all across the Pulo do Lobo domain; the resulting macrostructure is displayed in Fig. 1 (see also Pérez-Cáceres et al., 2015).

10. Timing of deformations and associated metamorphism in the Pulo do Lobo domain. Regarding timing of deformations, the reviewer bases his argument on the ages and deformations recorded by the Gil Márquez pluton. According to him, the lack of deformation in the older mafic facies (354 Ma) implies that the two first penetrative deformations in the Pulo do Lobo domain are older than 354 Ma and therefore they did not affect the Santa Iría Fm. However, the mafic rocks of the Gil Márquez pluton constitute a highly competent body, which is a poor marker for superposed deformations, as demonstrated by the fact that a younger felsic facies of this pluton (345 Ma) is foliated while the older one is isotropic. By contrast, our statements about the Santa Iría Fm are: i) its age is early Carboniferous according to discussion in point 3; and ii) it is affected by two penetrative deformations, as demonstrated by a detailed and comprehensive structural analysis (see point 9). Thus, only the first penetrative deformation of the Pulo do Lobo domain is Devonian (Late Devonian) in age, while the two subsequent deformations are Carboniferous (as also noted previously by Silva et al., 1990; line 211). Accordingly, the same timing applies to the syn-kinematic metamorphism associated with the first and second penetrative deformations of the Pulo do Lobo domain.

Regarding the third deformation (D3; upright folding), we already described a spaced and disjunctive crenulation cleavage S3 (lines 189-191, 202), which did not entail phyllosilicate growth (lines 399-400). This has been stressed in section 5.1 (lines 510-511), and no further implications are attained about D3.

11. The Gil Márquez pluton as evidence of active subduction. The calc-alkaline geochemistry of the Gil Márquez rocks is taken by the reviewer as evidence of active subduction at early Carboniferous time. The reviewer views this as a support to the subduction-related accretionary prism interpretation of the Pulo do Lobo domain. We believe, however, that these geochemical features are overrated when used to make inferences of active subduction at early Carboniferous time. Actually, the volume of the Gil Márquez rocks is very scarce to attest a magmatic arc, and, more importantly, the calc-alkaline geochemistry may be obtained from the residual mantle contaminated by the Devonian subduction, which at the time of Gil Márquez intrusion was no longer active. Indeed, there is regional evidence that collision started at Late Devonian time (e.g. Ponce et al., 2012 and references therein).

12. Writing corrections have been introduced in the revised version of the manuscript (lines 103, 136, 143, 234, 562).

To sum up and leaving aside the particular questions addressed above, the main concern of the reviewer is about the identification of the Pulo do Lobo lower formations (Pulo do Lobo and Ribeira de Limas Fms) with a subduction-related accretionary prism, an interpretation that we defy in our paper. If not used in a vague way (a usage that we do not endorse), an accretionary prism is a tectonic unit made up of a package of imbrications, having at least one of the two following key features: i) HP metamorphism indicative of subduction; ii) tectonic slices of mafic rocks and ocean floor sediments scrapped off from oceanic crust. None of these features is present in the lower formations of the Pulo do Lobo domain, according to the structural, radiometric and metamorphic data reported in our paper. Accordingly, we claim that: i) the structure is dominated by folding, despite local imbrications (see Fig. 1.c.2); ii) the mafic rocks embedded in the Pulo do Lobo Fm are dated at early Carboniferous age, thus being imbricated with Middle-Upper Devonian sediments and not representing slices of oceanic crust; and iii) the metamorphic gradient of these rocks is of low-pressure, as demonstrated by our detailed metamorphic study. Therefore, we maintain our conclusion that the Pulo do Lobo lower formations constitute a tectonic unit located very near the subduction/collision OMZ/SPZ boundary, but without the most typical features of a subduction-related accretionary prism.

Reply to the interactive comment of referee#2 on the paper entitled “Deciphering the metamorphic evolution of the Pulo do Lobo metasedimentary belt (SW Iberian Variscides)” by Irene Pérez-Cáceres et al. (Manuscript number se-2019-143).

1. General comments: We acknowledge the revision and positive comments of the anonymous referee 2. We also appreciate his/her constructive suggestions, which have contributed to improve the revised version of the manuscript.

2. Specific comments: All of the suggestions and corrections have been attended, as explained below point-by-point (line numbers in brackets correspond to the revised version of the manuscript with tracked changes (uploaded as supplement file to this response)):

Lines 48-49: the range of celadonite content and average data of b-cell dimension have been included in the abstract (lines 49-50 in the revised manuscript) and in the second paragraph of section 4.2 (lines 426, 431-432).

As for the keywords, “X-Ray diffraction” has been substituted by “Illite crystallinity”.

Line 100 (103): “allows to know” instead of “allows know”, as suggested.

In lines 163, 167 and 181 (174, 178, 192), “which” has been included after each formation is named, since these sentences are subordinated.

Line 228 (244-245): “SEM” has been changed to “scanning electron microscope (SEM)”, because this is the first time that is mentioned.

Line 276 (292-293): we refer here to the temperature of formation of white-mica, and it has been included according to the suggestion made by the referee.

Lines 292-294 (308-310): minerals and synthetic oxides have been rewritten with lowercases in the revised version.

Lines 318-321 (lines 337-339): regarding the EPMA analysis at the University of Huelva, information about the standards used and the analysis time has been incorporated in section 3.2.

Lines 324-330 (342-348 in the revised version) have been shortened following the referee’s suggestion. In addition, “carbonaceous material” has been abbreviated to “CM”.

Lines 341-344 (360-361): we have included justification of sample rejection for analysis.

Line 349 (368): “equipped” instead of “equiped”.

Line 361 (379): “Acording to SEM analysis” has been replaced by “According to the petrographic study”.

Line 369-370 (lines 387-388): The last sentence in the introduction to section 4 has been deleted, as suggested.

Line 373 (391): “of K-white mica” has been included.

Lines 374-376: The referee suggests adding a column in Table 1 with the KI values corresponding to the bulk fraction of the samples. Actually, this column was already included in the first version.

Lines 393-394 (411-412 of the revised manuscript): we agree with the referee comment. “very low to” and “presence of C/S and” have been deleted according to the referee’s correction.

Line 395 (413-414): we have specifically clarified the term “low-pressure gradient” according to Guidotti and Sassi (1986). Also clarified at the end of the abstract (“low pressure/temperature gradient”; line 51).

Line 409 (428): “illite” has been replaced by “illitic-mica”.

Line 412 (431-432): the values of low b-cell parameter and high d001 have been indicated.

Lines 419-420 (438-439): an assertion and reference have been incorporated to justify why poor-sudoite chlorites are related to higher temperatures.

Line 444 (463): the average temperature range has been revised.

Line 445-447 (465-467): the sentence “Nevertheless, the Bourdelle thermometer predicts temperatures up to 380-400°C” has been deleted because it is not significant as the referee explains. Other writing suggestions have also been taken into account.

Line 455 (476): Fig. 3 is now cited here.

Line 469 (489-492): the sentence has been changed as the referee suggests.

Lines 471-473 (492-494): location of Table 2: the last sentence of the first paragraph in section 5.1 has been moved to section 5.3 (600-602) as the referee suggests.

Line 481 (502): “our” has been substituted by “these”.

Line 498 (520-521): according to Abad et al. (2006), the KI value $0.14 \Delta^2\theta$ is the limit of high epizone conditions.

Line 512 (535-536): temperature ranges have been revised, giving the overall range based on the three approaches.

Line 513 (537): Fig. 4d is cited now.

Line 529 (552): “is difficult” has been substituted by “is really difficult”.

Lines 531-532 (554-555): “white mica crystallinity and” has been deleted according to the referee’s revision.

Lines 554-561 (597-604): In these sentences, there are some references on how igneous bodies (especially dykes or plutons) can influence the CM temperatures. The referee asks whether or not dykes really crop out in the studied area. As stated some lines above in the text (and in the geological description), the Pulo do Lobo contains layered mafic intrusions and some granitic plutons that could have enhanced the CM temperature in some samples (eg., sample PLB-93; see also lines 514-519 of the first version).

Line 567 (593): potassium feldspar (Fsp) has been incorporated.

Figure 1 caption (687): “and collected samples” has been added.

Figure 7: the referee asks why the width of the columns in Fig. 7a and Fig. 7b are different; the software used unfortunately does not allow changing it.

Table 1 and Figure 1: colour bar: The colour bars (“cold” to “hot” colours as temperature increases) have the only purpose of visual appearance of relative temperatures. To avoid confusion, different coloured bars were used for KI (from green to orange) and RSCM (from blue to red) parameters.

Table 1 caption: “Basel” has been incorporated to “KI values” (732). “Feldespar” has been substituted by “Feldspar” (734).

Table 1: the number of decimals are now equal. “KI colour” of sample 82 has been corrected.

References:

- Abad, I., Nieto, F., Gutiérrez-Alonso, G., Campo, M. D., López-Munguira, A., and Velilla, N.: Illitic substitution in micas of very low-grade metamorphic clastic rocks. *European Journal of Mineralogy*, 18(1), 59-69, 2006.
- Apalategui, O., Barranco, E., Contreras, F., Delgado, M., and Roldán, F. J.: Hoja 916, Aroche, Mapa Geológico de España a escala 1:50000, Inst. Geológico y Minero de España, Madrid, 1983.
- Braid, J. A., Murphy, J. B., Quesada, C., and Mortensen, J.: Tectonic escape of a crustal fragment during the closure of the Rheic Ocean: U–Pb detrital zircon data from the Late Palaeozoic Pulo do Lobo and South Portuguese zones, southern Iberia, *Journal of the Geological Society*, 168(2), 383-392, 2011.
- Guidotti, C.V., and Sassi, F.P.: Classification and correlation of metamorphic facies series by means of muscovite b data from low-grade metapelites, *Neues Jahrbuch fur Mineralogie-Abhandlungen*, 153, 363-380, 1986.

Lopes, G., Pereira, Z., Fernandes, P., Wicander, R., Matos, J.X., Rosa, D., and Oliveira, J.T.: The significance of reworked palynomorphs (middle Cambrian to Tournaisian) in the Visean Toca da Moura Complex (South Portugal). Implications for the geodynamic evolution of Ossa Morena Zone, *Rev. Palaeobot. Palynol.*, 200, 1-23, 2014.

Pérez-Cáceres, I., Martínez Poyatos, D., Simancas, J.F., and Azor, A.: The elusive nature of the Rheic Ocean in SW Iberia, *Tectonics*, 34, 2429-2450, 2015.

Pérez-Cáceres, I., Martínez Poyatos, D., Simancas, J.F., and Azor, A.: Testing the Avalonian affinity of the South Portuguese Zone and the Neoproterozoic evolution of SW Iberia through detrital zircon populations, *Gondwana Research*, 42, 177-192, 2017.

Pereira, Z., Fernandes, P., Matos, J., Jorge, R., and Oliveira, J.T.: Stratigraphy of the Northern Pulo do Lobo Domain, SW Iberia Variscides: A palynological contribution, *Geobios*, 51, 491-506, 2018.

Pereira, Z., Fernandes, P., Matos, J. X., Jorge, R. C. and Oliveira, J.T.: Reply to "Comment on «Stratigraphy of the Northern Pulo do Lobo Domain, SW Iberia Variscides: A palynological contribution» by Zélia Pereira et al. (2018)–*Geobios* 51, 491–506". *Geobios*, 55, 107-110, 2019.

Pereira, M.F., Martínez Poyatos, D., Pérez-Cáceres, I., Gama, C., and Azor, A.: Comment on "Stratigraphy of the Northern Pulo do Lobo Domain, SW Iberia Variscides: A palynological contribution" by Pereira, Z. et al. (2018) - *Geobios*, 51, 491-506. *Geobios*, in press, 2019.

Ponce, C., Simancas, J.F., Azor, A., Martínez Poyatos, D.J., Booth-Rea, G., and Expósito, I.: Metamorphism and kinematics of the early deformation in the Variscan suture of SW Iberia, *Journal of Metamorphic Geology*, 30(7), 625-638, 2012.

Silva, J. B., Oliveira, J.T., and Ribeiro, A.: South Portuguese Zone, structural outline, in: *Pre-Mesozoic Geology of Iberia*, edited by: Dallmeyer, R.D., and Martínez García, E., Springer, Berlin, Germany, pp. 348-362, 1990.

1 **Deciphering the metamorphic evolution of the Pulo do**
2 **Lobo metasedimentary beltdomain (SW Iberian**
3 **Variscides)**

4
5 Irene Pérez-Cáceres¹, David Jesús Martínez Poyatos¹, Olivier Vidal², Olivier Beysac³,
6 Fernando Nieto⁴, José Fernando Simancas¹, Antonio Azor¹ and Franck Bourdelle⁵

7
8 1 Departamento de Geodinámica, Facultad de Ciencias, Universidad de Granada, Campus de
9 Fuentenueva s/n, 18071 Granada, Spain.

10 2 Institut de Sciences de la Terre (ISTerre), CNRS-University of Grenoble 1, 1381 rue de la Piscine,
11 38041 Grenoble, France.

12 3 Institut de Physique des Matériaux et de Cosmochimie (IMPMC), CNRS-Sorbonne Université,
13 Case Courrier 115, 4 place Jussieu, 75005 Paris, France.

14 4 Departamento de Mineralogía y Petrología, IACT, Facultad de Ciencias, Universidad de Granada-
15 CSIC, Campus de Fuentenueva s/n, 18071 Granada, Spain.

16 5 Laboratoire Génie Civil et géo-Environnement (LGCgE), Université de Lille, Bât. SN5, Cité
17 Scientifique, 59655 Villeneuve d'Ascq, France

18 Correspondence to: Irene Pérez-Cáceres (perezcaceres@ugr.es)

Con formato: Español (España)

19
20
21 **Abstract**

22 The Pulo do Lobo beltdomain is one of the units related to the orogenic suture between the
23 Ossa-Morena and the South Portuguese zones in the SW Iberian Variscides. This
24 metasedimentary unit has been classically interpreted as a Rheic subduction-related
25 accretionary prism formed during the pre-Carboniferous convergence and eventual collision
26 between the South Portuguese Zone (part of Avalonia) and the Ossa-Morena Zone (peri-
27 Gondwanan terrane). Discrete mafic intrusions also occur in the dominant Pulo do Lobo
28 metapelites, related to an intraorogenic Mississippian transtensional and magmatic event that
29 had a significant thermal input. Three different approaches have been applied to the
30 Devonian/Carboniferous phyllites and slates of the Pulo do Lobo beltdomain in order to
31 study their poorly known low-grade metamorphic evolution. X-Ray diffraction (XRD) was
32 used to unravel the mineralogy and measure crystallographic parameters (illite “crystallinity”
33 and K-white mica *b*-cell dimension). Compositional maps of selected samples were obtained
34 from electron probe microanalysis, which allowed processing with XmapTools software, and
35 chlorite semi-empirical and thermodynamic geothermometry was performed. Thermometry

36 based on Raman spectroscopy of carbonaceous material (RSCM) was used to obtain peak
37 temperatures.

38 The microstructural study shows the existence of two phyllosilicate growth events at the
39 chlorite zone, the main one (M_1) related to the development of a Devonian foliation S_1 , and
40 a minor one (M_2) associated with a crenulation cleavage (S_2) developed at middle/upper
41 Carboniferous time. M_1 entered well into epizone (greenschist facies) conditions. M_2
42 conditions were at lower temperature, reaching the anchizone/epizone boundary. These data
43 accord well with the unconformity that separates the Devonian and Carboniferous
44 formations of the Pulo do Lobo ~~belt~~domain. The varied results obtained by the different
45 approaches followed, combined with microstructural analysis, are indicative of different
46 snapshots of the metamorphic history. Thus, RSCM temperatures are higher in comparison
47 with the other methods applied, which is interpreted as reflecting a faster reequilibration
48 during the short-lived thermal Mississippian event. Regarding the metamorphic pressure, the
49 data are very homogeneous ~~to~~ very low celadonite content (0-10 %) in muscovite (and low
50 values of K-white mica *b*-cell dimension 8.995 Å mean value), indicating a low-
51 pressure/temperature gradient, which is unexpected in a subduction-related accretionary
52 prism.

53

54 **Keywords**

55 Pulo do Lobo metapelites

56 Low-pressure gradient

57 ~~X-Ray diffraction~~

58 Illite “crystallinity”

59 Chlorite geothermometry

60 Raman spectroscopy of carbonaceous material

61

62 **Highlights**

63 A multidisciplinary approach has been applied to study the metamorphism of the Pulo do
64 Lobo metapelites.

65 Devonian metamorphism entered epizone conditions.

66 Carboniferous metamorphism reached the anchizone/epizone boundary.

67 The inferred low-pressure gradient is incompatible with a subduction-related accretionary
68 prism.

69 1. Introduction

70 The knowledge of temperature and pressure conditions reached by the low-grade
71 metasedimentary units stacked hinterlands of orogens helps to better interpret their
72 tectonometamorphic evolution (e.g., Goffé and Velde, 1984; Franceschelli et al., 1986; Ernst,
73 1988; Gutiérrez-Alonso and Nieto, 1996; Frey and Robinson, 1999; Bousquet et al., 2008;
74 Lanari et al., 2012). In this regard, the various results derived from the application of diverse
75 geothermometric and/or geobarometric methods may also allow the identification and
76 characterization of superposed tectonometamorphic events, thus improving the knowledge
77 of the P-T paths and their tectonic significance (e.g., Brown, 1993; Crouzet et al., 2007; Ali,
78 2010; Lanari et al., 2012; Airaghi et al., 2017).

79 The metamorphism of the Iberian Variscides has been mostly studied on intensely
80 metamorphosed rocks in order to characterize high-grade events and obtain the P-T-t paths
81 of suture-related units (e.g., Gil Ibarra et al., 1990; Abalos et al., 1991; Escuder Viruete et
82 al., 1994; Barbero, 1995; Arenas et al., 1997; Fonseca et al., 1999; López-Carmona et al., 2013;
83 Martínez Catalán et al., 2014). The low- to very low-grade units have been also studied (e.g.,
84 Martínez Catalán, 1985; Bastida et al., 1986, 2002; López Munguira et al., 1991; Gutiérrez-
85 Alonso and Nieto, 1996; Abad et al., 2001, 2002, 2003a; Martínez Poyatos et al., 2001; Nieto
86 et al., 2005; Vázquez et al., 2007), despite the scarcity of appropriate robust methodologies
87 to apply in these kind of rocks. Obtaining new results from the low-grade rocks of the Pulo
88 do Lobo [belt domain](#), a suture-related low-grade unit in SW Iberia, is of capital importance
89 in order to understand its significance and tectonometamorphic evolution, that have been
90 cause of discrepancies, and to reconstruct the overall history of the SW Iberian Variscides.

91 In this work, three different methodologies are applied to a number of samples of the Pulo
92 do Lobo [belt domain](#) (Fig. 1): (i) X-Ray Diffraction (XRD) in order to identify minerals not
93 easily recognizable with optical microscopy (fine-grained muscovite, paragonite, mixed-layer
94 phyllosilicates, etc.) and obtain thermobarometric information via the measurement of
95 crystallographic parameters (illite “crystallinity” and *b*-cell dimension); (ii) Compositional
96 maps derived from electron probe microanalysis (EPMA), which enable the recognition of
97 different tectonometamorphic events by combining mineral composition and microtextural
98 features (e.g., Airaghi et al., 2017), as well as the application of geothermobarometers based
99 on chlorite and K-white mica compositions; and (iii) Raman spectroscopy of carbonaceous
100 material (RSCM) to estimate peak temperatures thanks to an adapted thermometric
101 calibration. Firstly, the results obtained enables discussing the tectonometamorphic
102 evolution of the Pulo do [BeltLobo domain](#). Moreover, the comparison of the different
103 approaches allows [to](#) know further their reliability and sensitivity to characterize different
104 geological processes.

105

106 2. Geological setting

107 The SW Iberian Variscides resulted from the Devonian-Carboniferous left-lateral oblique
108 collision of three different terranes: the Central Iberian Zone (CIZ), the Ossa-Morena Zone
109 (OMZ) and the South Portuguese Zone (SPZ) (Fig. 1a). The boundaries between these
110 terranes are considered as orogenic sutures (e.g., [Quesada, 1990; Pérez-Estaún and Bea, 2004;](#)

111 Pérez-Cáceres et al., 2016, ~~and references therein~~). Besides the dominant left-lateral
112 shortening kinematics, SW Iberia also attests Mississippian synorogenic sedimentary basins,
113 widespread mafic magmatism and high-temperature metamorphic areas, which altogether
114 reveal an intraorogenic transtensional stage (Simancas et al., 2003, 2006; Pereira et al., 2012;
115 Azor et al., 2019).

116 The OMZ is commonly interpreted as a continental piece that drifted from the CIZ (i.e.,
117 north Gondwana) in early Paleozoic times (Matte, 2001). The OMZ/CIZ suture (Badajoz-
118 Córdoba Shear Zone) includes early Paleozoic amphibolites with oceanic affinity, eclogite
119 relicts and intense high- to low-grade left-lateral shear imprint (Burg et al., 1981; Abalos et
120 al., 1991; Azor et al., 1994; Ordóñez-Casado, 1998; López Sánchez-Vizcaíno et al., 2003;
121 Pereira et al., 2010). Ediacaran to Carboniferous sedimentary successions with an
122 unconformity at the base or the Lower Carboniferous characterize the OMZ. Low-grade
123 regional metamorphism dominates the OMZ, though there are areas of high-temperature /
124 low-pressure metamorphism associated with Early Carboniferous magmatism (e.g. Bard,
125 1977; Crespo-Blanc, 1991; Díaz Azpiroz et al., 2006; Pereira et al., 2009).

126 The SPZ is a continental piece considered as a fragment of Avalonia (~~Pérez-Cáceres et al.,
127 2017, and references therein~~). ~~Thus, thus~~ the OMZ/SPZ boundary is usually interpreted as
128 the Rheic Ocean suture (~~Crespo-Blanc and Orozco; 1988; Eden and Andrews, 1990; Silva et
129 al., 1990; Quesada et al., 1994; Braid et al., 2011; Pérez-Cáceres et al., 2015 and references
130 therein, 2017~~). This boundary is delineated by the Beja-Acebuches Amphibolites (Fig. 1b), a
131 narrow strip of metamafic rocks that resembles a dismembered ophiolitic succession (from
132 greenschists to metagabbros and locally ultramafic rocks) (e.g., Bard, 1977; Crespo-Blanc,
133 1991; Quesada et al., 1994). This unit was interpreted as a Rheic ophiolite (Munhá et al.,
134 1986; Crespo-Blanc, 1991; Fonseca and Ribeiro, 1993; Quesada et al., 1994; Castro et al.,
135 1996), though this idea was reconsidered based on the Mississippian age of the mafic
136 protholites (≈ 340 Ma; Azor et al., 2008). ~~Actually~~ At present, the Beja-Acebuches unit is better
137 interpreted as an outstanding evidence of the early Carboniferous intraorogenic, lithospheric-
138 scale transtensional and magmatic episode that here obscures the previous suture-related
139 features of the OMZ/SPZ boundary (Pérez-Cáceres et al., 2015 and references therein).
140 Nevertheless, there is also the alternative explanation that the OMZ/SPZ boundary was a
141 protected tract of Rheic oceanic lithosphere that did not close until Carboniferous time
142 (Murphy et al., 2016; Braid et al., 2018; Quesada et al., 2019). The rocks of the Beja-
143 Acebuches Amphibolites were affected by a left-lateral ductile shearing that occurred at
144 granulite to greenschist facies conditions, though amphibolite facies conditions were
145 dominant (e.g., Quesada et al., 1994; Castro et al., 1996; Castro et al., 1999; Díaz Azpiroz et
146 al., 2006). This metamorphism has been dated at 345-330 Ma (Dallmeyer et al., 1993; Castro
147 et al., 1999), thus suggesting that it started very shortly after the magmatic emplacement.

148 North of the Beja-Acebuches Amphibolites, the allochthonous Cubito-Moura unit might be
149 the only witness of the Rheic Ocean suture (Fonseca et al., 1999; Araújo et al., 2005; Pérez-
150 Cáceres et al., 2015). This unit was emplaced onto the southern OMZ border (Fig. 1b) with
151 a left-lateral top-to-the-ENE kinematics (Ponce et al., 2012). It contains Ediacaran-Lower
152 Paleozoic metasediments and Ordovician MORB-featured mafic rocks (≈ 480 Ma; Pedro et
153 al., 2010) transformed into high-pressure blueschists and eclogites at ≈ 370 Ma (Moita et al.,
154 2005). The high-pressure metamorphism has also been studied by using white mica and

155 chlorite (and chloritoid pseudomorphs) mineral equilibria (Booth-Rea et al., 2006; Ponce et
156 al., 2012; Rubio Pascual et al., 2013), yielding peak conditions of 1 GPa at 450 °C.

157 South of the Beja-Acebuchos Amphibolites, low- to very low-grade successions crop out ~~in~~
158 ~~the SPZ~~: Devonian siliciclastics, earliest Carboniferous volcano-sedimentary rocks, and a
159 south-migrating Carboniferous flysch (e.g., Oliveira, 1990). ~~The SPZ can be divided, from~~
160 ~~north to south~~; ~~These rocks are usually grouped~~ into two geological domains: the Pulo do
161 Lobo ~~belt (see below)~~, ~~domain to the Iberian Pyrite belt (that includes massive sulphide~~
162 ~~deposits)~~ north, and the Carboniferous flysch, SPZ s. str. to the south (Fig. 1a, b). The
163 deformation in the SPZ consists in a south- to southwest-vergent fold and thrust belt with
164 decreasing strain intensity and age southwards (Oliveira, 1990; Simancas et al., 2004). The
165 metamorphic grade also decreases southwards, from epizone to diagenesis, through the SPZ
166 (Munhá, 1990; Abad et al., 2001). The Pulo do Lobo domain, which has been traditionally
167 considered as a suture-related unit (see below) is the focus of this work.

168

169 2.1. Pulo do Lobo ~~belt~~domain

170 ~~The northernmost unit of the SPZ is the Pulo do Lobo belt, whose evolution is intimately~~
171 ~~related to the OMZ/SPZ suture (Fig. 1b).~~ ~~The Pulo do Lobo belt~~ The Pulo do Lobo domain
172 constitutes a polydeformed structure affecting low-grade Devonian-Carboniferous
173 sedimentary formations. These formations are, from bottom to top (Fig. 1b-c):

174 (i) The Pulo do Lobo formation (s. str.), which is constituted by a succession of satiny black
175 to grey phyllites and fine-grained schists with minor intercalations of quartz sandstones (Fig.
176 2a). The presence of abundant segregated quartz veins (pre- to post-folding) is common. The
177 palynological content suggests a middle Frasnian age (Pereira et al., 2018).

178 (ii) The Ribeira de Limas formation, which is constituted by phyllites with thin beds of quartz
179 sandstones and arkoses (Fig. 2b). The presence of palynomorphs also suggests a middle
180 Frasnian age for this formation (Pereira et al., 2018). The contact with the underlying Pulo
181 do Lobo formation is gradual, with a progressive increase of sandstones and a decrease of
182 phyllites upwards. For that reason, we will refer to the Pulo do Lobo and Ribeira de Limas
183 formations as the lower formations of the Pulo do Lobo ~~belt~~domain. Furthermore, these
184 lower formations share the same structure consisting in three fold-related foliations (Fig. 2a-
185 b; Pérez-Cáceres et al., 2015). The first foliation of the lower formations (S_1) is preserved
186 inside microlithons of the second foliation (S_2); usually, the angle between these two
187 foliations is high. S_2 is the main foliation and consists in a crenulation-dissolution cleavage
188 that frequently appears as a milimetric- to centimetric-spaced tectonic banding. This foliation
189 is axial-plane to north-vergent folds. The third foliation (S_3) is a spaced crenulation-
190 dissolution cleavage that sometimes develops a characteristic decimetric- to metric-scale
191 tectonic banding. S_3 is associated with upright to slightly south-vergent folds.

192 (iii) The Santa Iria formation, which is composed by alternating beds of slates and greywackes
193 (Fig. 2c). The greywacke beds show normal grading and erosive base. Paleontological and
194 palynostratigraphic studies suggest an Upper Famennian age for this formation (Pereira et
195 al., 2008; 2018). However, an early Carboniferous age is much plausible, since more than
196 90% of the palynomorphs correspond to reworked material (Lopes et al., 2014) and the

197 younger detrital zircon population is early Carboniferous (Braid et al., 2011; Pérez-Cáceres
198 et al., 2017; Pereira et al., 2019). The Santa Iría formation only shows two foliations,
199 correlative with the last two deformation phases in the lower formations. Therefore, an
200 unconformity between them is inferred, which also agrees with the age and flysch character
201 of the Santa Iría formation (Pérez-Cáceres et al., 2015). S₂ is observed as a penetrative slaty
202 cleavage, while S₃ is a disjunctive crenulation cleavage.

203 According to ~~the evolutionary model proposed by Silva et al. (1990) and~~ Pérez-Cáceres et al.
204 (2015), the two main foliations (S₂ and S₃) in the Pulo do Lobo ~~belt domain~~ resulted from the
205 middle/upper Carboniferous collision between the OMZ and SPZ. On the contrary, the first
206 foliation (S₁) in the Pulo do Lobo ~~belt domain~~ might have formed during the vanishing stages
207 of Rheic Ocean subduction and/or the starting Variscan collision, probably at Late Devonian
208 time.

209 The Pulo do Lobo ~~belt domain~~ contains some decimetric- to metric-scale lenticular bodies of
210 MORB-featured metamafic rocks ~~intercalated within. At some outcrops, the mafic rocks are~~
211 ~~embedded in a greenish detrital matrix, thus suggesting an olistostromic origin (the Peramora~~
212 ~~Olistostrome; Eden and Andrews, 1990). These rocks are tectonically imbricated with~~ the
213 phyllites of the Pulo do Lobo formation and ~~interpreted as hence forming~~ a tectonic mélange
214 (the so-called Peramora Mélange; Fig. 1b-c; ~~Apalategui et al., 1983;~~ Eden, 1991; Dahn et al.,
215 2014). Based on this aspect and on the supposedly Rheic Ocean derived greenschists, the
216 Pulo do Lobo ~~belt domain~~ has been classically interpreted as a pre-collisional subduction-
217 related accretionary prism (Eden and Andrews, 1990; Silva et al., 1990; Eden, 1991; Braid et
218 al., 2010; Ribeiro et al., 2010; Dahn et al., 2014); ~~Quesada et al., 2019). However, the recently~~
219 obtained Mississippian U/Pb zircon ages from the metamafic rocks (Dahn et al., 2014; Pérez-
220 Cáceres et al., 2015) make difficult to maintain such hypothesis. More properly, they can be
221 interpreted as mafic intrusions/extrusions in the frame of the intraorogenic transtensional
222 magmatic event that prevailed in SW Iberia during the Mississippian. The metamafic rocks
223 display a foliation (equivalent to the S₂ of the enveloping metasediments) developed at loosely
224 constrained greenschist facies conditions. These rocks would have been imbricated with the
225 Pulo do Lobo metasediments during the second deformation phase which caused S₂
226 ~~(Peramora Olistostrome; Pérez-Cáceres et al., 2015). Our multidisciplinary metamorphic~~
227 study of the Pulo do Lobo metasediments provides with crucial data concerning the tectonic
228 significance of this ~~belt domain~~.

229

230 3. Samples and analytical methods

231 Eighteen samples were collected from well-exposed outcrops of phyllosilicate-rich detrital
232 rocks of the Pulo do Lobo ~~belt domain~~ along two north-south transects perpendicular to the
233 structural trend. Five samples belong to the Santa Iría formation (unconformable upper
234 formation) and thirteen to the lower formations (~~Pulo do Lobo and Ribeira de Limas~~
235 ~~formations) (location of samples are in the map and cross-sections of Fig. 1b-c and the UTM~~
236 coordinates in supplementary information). As a whole, the samples were selected in ~~not~~
237 ~~non-~~altered outcrops, far from faults and joints, and were taken as homogeneous as possible.
238 Sampling design was intended to collect representative sites, both of the overall stratigraphic
239 succession and along the two transects. We also aimed to characterize the unconformity

240 between the lower and upper formations from a metamorphic point of view, since
241 “crystallinity” aspect at first sight seems to be lower in the Santa Iría formation. Some
242 samples from the lowermost Pulo do Lobo formation were collected not far from the
243 metabasite lenses of the Peramora Mélange.

244 Samples were examined under the optical microscope and [SEMscanning electron](#)
245 [microscope \(SEM\)](#) for overall mineralogy, deformation and minerals/ foliations relationships
246 using an environmental scanning electron microscope FEI model Quanta 400, operating at
247 15–20 keV (Centro de Instrumentación Científica-CIC, University of Granada, Spain).

248

249

250 3.1. X-Ray diffraction

251 Sample preparation and analysis by XRD were done in the laboratories of the Department
252 of Mineralogy and Petrology of the University of Granada (Spain). After washing and
253 cleaning of patinas and oxides, samples were crushed to a <2 mm fraction. The <2 μm
254 fractions were separated by repeated extraction of supernatant liquid after centrifugation,
255 according to the Stokes' law. Oriented aggregates were prepared by sedimentation on glass
256 slides of whole-rock and <2 μm fractions (the latter aims to minimize the content of detrital
257 micas non-re-equilibrated during very low-grade metamorphism, which are generally larger
258 than 2 μm ; Moore and Reynolds, 1997). Samples were also treated with ethylene glycol
259 (EGC) to identify illite/smectite or chlorite/smectite mixed-layers on the basis of their
260 expansibility. Samples were analyzed using a PANalytical X'Pert Pro powder diffractometer
261 equipped with an X'Celerator detector, $\text{CuK}\alpha$ radiation, operated at 45 kV and 40mA, Ni
262 filter and 0.25° divergence slit. The resulting diffraction diagrams were examined to extract
263 information on mineralogy based on their characteristic reflections and white mica crystal
264 data.

265 The Illite “Crystallinity” index (Kübler Index; KI; Kübler, 1968) has been estimated from
266 the measurement of the full peak-width of K-white mica at half maximum intensity (FWHM
267 values), expressed as $\Delta^{\circ}2\theta$ of the Bragg angle. Preparation of samples and experimental
268 conditions were carried out according to IGCP 294 IC Working Group recommendations
269 (Kisch, 1991). A step increment of 0.008° 2θ and a counting time of 52 s/step were used in
270 the diffractometer. The KI has been measured in all samples for both the 5 and 10 Å
271 reflection peaks of K-white mica in order to identify possible effects of other overlapping
272 phases (Nieto and Sánchez-Navas, 1994; Battaglia et al., 2004). Some XRD traces showing
273 complex mixture of mixed-layered minerals were decomposed with the MacDiff software
274 (Petschick, 2004). The FWHM values obtained in the laboratory (x) have been transformed
275 to Crystallinity Index Standard (CIS) values (y) using the equation $y=0.972x + 0.1096$ ($R^2 =$
276 0.942), obtained from the measure in our lab of the international standards of Warr and Rice
277 (1994). Finally, they have been expressed in term of traditional KI values using the equation
278 of Warr and Ferreiro Mähnlmann (2015; ‘CIS’ = 1.1523*Kübler index ‘Basel lab’ + 0.036).
279 The lower and upper boundaries of the anchizone in the KI scale are 0.42 and 0.25 °2 θ ,
280 respectively (Warr and Ferreiro Mähnlmann, 2015). The thermal range for the anchizone is

281 estimated in c. 200-300 °C, though the KI cannot be considered as a true geothermometer
282 (Frey, 1987; Kisch, 1987).

283 The *b*-cell parameter of white mica was obtained from the (060) reflection peak measured
284 with quartz as internal standard on polished rock-slices cut normal to the sample main
285 foliation (Sassi and Scolari, 1974). The *b*-cell dimension of K-white mica is often proportional
286 to the magnitude of phengitic substitution and therefore considered as a proxy of the
287 pressure conditions during its crystallization. Thus, Guidotti and Sassi (1986) have shown
288 that *b* values lower than 9.000 Å are typical of low-pressure facies conditions, while *b* values
289 higher than 9.040 Å are related to rather high-pressure facies metamorphism. Precise
290 measurements of the basal spacing of white mica (d_{001}) have also been made, using quartz
291 from the sample itself as internal standard. d_{001} is related to the paragonitic Na/K substitution
292 (Guidotti et al., 1992), thereby approximately reflecting the temperature of [white-mica](#)
293 formation (Guidotti et al., 1994).

294

295 3.2. EPMA-derived X-Ray compositional maps and chlorite thermometry

296 From all of the collected samples, we selected those with the larger phyllosilicate grain-size
297 for electron probe microanalysis (EPMA). Thus, three carbon-coated polished thin-sections
298 were studied. The selected samples (PLB-84, PLB-88 and PLB-93) belong to the lower
299 formations of the Pulo do Lobo [belt domain](#) (Fig. 2d-e). The Santa Iria samples could not be
300 studied due to the tiny grain size of the slaty minerals (commonly less than 3 µm).

301 Compositional maps and accurate spot analyses were performed on a JEOL JXA-8230
302 EPMA at the Institut des Sciences de la Terre (ISTerre) in Grenoble (France), according to
303 the analytical procedure proposed by de Andrade et al. (2006) and Lanari et al. (2014a). The
304 data acquisition was made in wavelength dispersive spectrometry mode (WDS). Ten
305 elements (Si, Ca, Al, K, Mn, Na, P, Ti, Fe and Mg) were analyzed using five WD
306 spectrometers: TAP crystal for Si and Al, PETL for Ti and P, TAPH for Na and Mg, PETH
307 for K and Ca, and LIFH for Mn and Fe. The standardization was made by using certified
308 natural minerals and synthetic oxides: [Wollastonite](#)[wollastonite](#) (Si, Ca),
309 [Corundum](#)[corundum](#) (Al), [Orthoclase](#)[orthoclase](#) (K), [Rhodonite](#)[rhodonite](#) (Mn), [Albite](#)[albite](#)
310 (Na), [Apatite](#)[apatite](#) (P), [Rutile](#)[rutile](#) (Ti), [Hematite](#)[hematite](#) (Fe), and [Periclase](#)[periclase](#) (Mg).
311 X-Ray maps were obtained by adding successive adjacent profiles. Beam current of 100 nA
312 and beam size spot (focused) were used. The step (pixel) size was 1 µm and dwell time was
313 200-300 msec per pixel. Spot analyses were obtained along the profiles within the mapping
314 at 15 kV accelerating voltage, 12 nA beam current and 2 µm beam size spot (focused). The
315 on-peak counting time was 30 sec for each element and 30 sec for two background
316 measurements at both sides of the peak. ZAF correction procedure was applied. The internal
317 standards were orthoclase and/or chromium-augite (Jarosewich et al., 1980), which were run
318 (3 points on each standard) after each profile in order to monitor instrumental drift and
319 estimate analytical accuracy. Drift correction was made, if necessary, using the corresponding
320 regression equation.

321 The WDS X-Ray maps were then processed with XMapTools
322 (<http://www.xmaptools.com>), a MATLAB©-based graphical user interface program to

323 process the chemical maps, link them to thermobarometric models and estimate the
324 pressure-temperature conditions of crystallization of minerals in metamorphic rocks (Lanari
325 et al., 2014a). The compositional maps were standardized with the spot analyses measured
326 along the profiles and mineral compositions were plotted into binary and ternary diagrams
327 using the interface modules *Chem2D* and *Triplot3D*. Chemical maps of amount of tetrahedral
328 aluminum (Al^{IV}) of chlorites were acquired, because is at the base of many empirical chlorite
329 thermometers (e.g. Cathelineau and Nieva, 1985; Cathelineau, 1988). The temperature
330 conditions were estimated for each chlorite pixel of the maps using the chlorite thermometer
331 of Lanari et al. (2014b), as well as the approaches of Vidal et al. (2006) and Bourdelle et al.
332 (2013), which are summarized in the supplementary information.

333 In addition to the above mentioned compositional maps, white micas from seven carbon-
334 coated thin sections of the lower formations of the Pulo do Lobo ~~belt~~domain were analyzed
335 before with a Jeol WDS four-spectrometer microprobe (JXA-8200 Superprobe) at the
336 University of Huelva (Spain). A combination of silicates and oxides were used for
337 calibration: ~~standards used were wollastonite (Si and Ca), potassium feldspar (Al, K and Na),~~
338 ~~forsferite (Mg) and fayalite (Fe).~~ Single point analyses were obtained with ~~4020~~ nA probe
339 current, 1-5 μ m spot size; and ~~2015~~ kV of acceleration voltage, ~~with 5 s counting times.~~

340

341 3.3. Raman Spectroscopy of carbonaceous material

342 ~~Beysac et al. (2002a) calibrated a technique for the quantification of peak metamorphic~~
343 ~~temperature, which can be used even in the absence of specific mineral assemblages~~
344 ~~necessary for classical thermobarometric estimates. This technique,~~ Raman Spectroscopy of
345 Carbonaceous Material (RSCM), is based on the observation that sedimentary carbonaceous
346 material (CM) is progressively transformed into graphite at increasing temperature. ~~Beysac~~
347 ~~et al. (2002a) found a linear relationship between temperature and the structural state of CM~~
348 ~~quantified by Raman microspectroscopy.~~ Because of the irreversible character of
349 graphitization, CM structure is not sensitive to the retrograde path during exhumation of
350 rocks, but only depends on the maximum temperature reached during metamorphism
351 (Beysac et al., 2002a). Temperature can be determined in the range 330-650°C with a
352 calibration-attached accuracy of ± 50 °C due to uncertainties on petrologic data used for the
353 calibration. Relative uncertainties on temperature are, however, much smaller (around 10-15
354 °C; Beysac et al., 2004). For temperature below 330 °C, Lahfid et al. (2010) performed a
355 systematic study of the evolution of the Raman spectrum of CM in low-grade metamorphic
356 rocks in the Glarus Alps (Switzerland). They showed that the Raman spectrum of CM is
357 slightly different from the spectrum observed at higher temperature and they established a
358 quantitative correlation between the degree of ordering of CM and temperature.

359 In this work, twelve representative thin-sections previously examined by optical microscopy
360 were selected. From them, ten samples were finally analyzed: ~~(according to their larger CM~~
361 ~~grain-size and content):~~ eight samples belong to the lower formations (Pulo do Lobo and
362 Ribeira de Limas formations), while the other two belong to the Santa Iría formation.
363 Polished thin-sections cut perpendicularly to the foliation were analyzed at the Institut de
364 Minéralogie, de Physique des Matériaux et de Cosmochimie at the Sorbonne University of
365 Paris (France). We followed closely the analytical procedure described by Beysac et al.

366 (2002a, b; 2003; see supplementary information). More than 15 Raman spectra (Fig. 3) were
367 obtained for each sample using a Renishaw InVIA Reflex microspectrometer
368 ~~equiped~~equipped with a 514.5 nm Modulaser argon laser under circular polarization. The
369 laser was focused by a DMLM Leica microscope, and laser power was set below 1 mW at
370 the sample surface. The Rayleigh diffusion was eliminated by edge filters and the signal was
371 dispersed using a 1800 g/mm grating and finally analyzed by a Peltier cooled RENCAM
372 CCD detector. The recorded spectral window was large to correctly set the background
373 correction, from 700 to 2000 cm^{-1} in case of low-temperature samples. Before each session,
374 the spectrometer was calibrated with a silicon standard. CM was systematically analyzed
375 behind a transparent adjacent mineral, generally quartz or white mica grains oriented along
376 S_1 . For a full description of the temperature calculations see the supplementary information.

377

378 4. Results

379 ~~According to SEM analysis~~According to the petrographic study, all the samples correspond
380 to slates or phyllites with phyllosilicates smaller than 500 μm , composed of variable quartz
381 + K-white mica \pm chlorite \pm feldspar \pm ore and accessory minerals (Fig. 2d-f). Samples from
382 the Santa Iría formation have much smaller grain-size and apparently lower “crystallinity”
383 (Fig. 2f). The first foliation S_1 is defined by the largest micas and chlorites (Fig. 2d-e), being
384 folded by microscopic- to centimetric-scale tight folds of the second deformation phase (Fig.
385 2a-b, d-e). The second foliation S_2 is the main foliation at outcrop (Fig. 2a-c), but the
386 development of phyllosilicates (mostly white mica) is lesser than S_2 . The third foliation S_3 is
387 much less penetrative (Fig. 2a-c) and does not develop phyllosilicates. ~~Large detrital~~
388 ~~phyllosilicate clasts have not been observed.~~

389

390 4.1. X-Ray diffraction

391 The mineralogy and crystal parameters of K-white mica obtained from the 18 samples of the
392 Pulo do Lobo ~~belt~~domain are summarized in Table 1. The results of KI values, b-cell
393 parameter and d_{001} analyzed in K-white mica, obtained from whole-rock and $<2 \mu\text{m}$ fractions
394 are very similar, which suggests that detrital micas re-equilibrated during metamorphism.

395 The mineralogy of the samples is relatively simple: Qz + Ms + Fsp+ Chl \pm Pg \pm C/S. The
396 slates of the Santa Iría formation have quartz, muscovite and chlorite, with chlorite/smectite
397 interlayers (C/S) in some samples. In the lower formations, besides quartz and muscovite,
398 chlorite is present in almost all of the samples, paragonite appears in most of them, and
399 chlorite/smectite interlayers are occasional.

400 KI values measured in the 10 Å peak of white mica from the $<2 \mu\text{m}$ fraction are shown in
401 Table 1 and Fig. 1c with a relative colour bar from orange (lower values) to green (higher
402 values). Values of the Santa Iría samples (n=5) range from 0.20 to 0.26 $\Delta^\circ 2\theta$, the mean value
403 being 0.23 (standard deviation 0.02). As for the lower formations (n=12), KI values range
404 from 0.17 to 0.22, the mean value being 0.19 (standard deviation 0.02). KI values measured
405 in the 5 Å peak (not shown) are very similar to those of the 10 Å peak.

406 The measured *b*-cell parameter of white mica varies in a close range around 9 Å (8.991-9.002).
407 Mean value is 8.995 Å (standard deviation 0.003) for the Santa Iría formation samples, and
408 8.997 Å (standard deviation 0.003) for the samples of the lower formations. d_{001} values
409 average 9.992 Å (standard deviation 0.004) and differ slightly between upper and lower
410 formations, being higher in the upper formation.

411 The results obtained through X-Ray diffraction denote ~~very low to~~ low-grade metamorphic
412 conditions due to the ~~presence of C/S and~~ KI values between 0.17-0.26 $\Delta^{\circ}2\theta$. In addition,
413 *b*-cell parameters ~~are lower than 9.000 Å which~~ show a low-pressure metamorphic gradient-
414 (low pressure/temperature metamorphic facies conditions; Guidotti and Sassi, 1986).

415

416 4.2. Compositional maps and chlorite thermometry

417 X-Ray maps show the distribution of major elements and allow identifying white mica,
418 chlorite, and some albite porphyroblasts, with ilmenite and rutile as accessory minerals (Fig.
419 4a-b). Although quartz is abundant in all of the samples, the zoomed selected areas for X-
420 ray mapping (composed mostly by phyllosilicates) do not contain quartz (Fig. 4a-b). White
421 mica is abundant along both S_1 and S_2 foliations (Fig. 2d-e and 4b). Chlorite is found mostly
422 along S_1 , being very scarce and small-sized along S_2 (Fig. 2e and 4b), with the exception of
423 sample PLB-93 where chlorite is similar in amount in both foliation domains (Fig. 4b).

424 Mapped compositions of end-members of white mica and chlorite have been plotted in the
425 ternary diagrams of Figure 5. The composition of white mica is similar in the three maps. It
426 is close to muscovite, with 25% of pyrophyllite and very scarce celadonite content (0-10%;
427 Fig. 5a). The high content of pyrophyllite (high amount of interlayer vacancies) is typical of
428 low-pressure ~~illitic-mica~~ compositions. Figure 6 shows white mica compositional ratios,
429 which can be related to P/T conditions: they present low degree of Na substitution and low
430 phengitic component, thus being close to the muscovite end-member. These results point to
431 low-pressure conditions and agree well with XRD results: low *b*-cell parameter (≤ 9.000 Å)
432 and high d_{001} (≥ 9.985 Å; Table 1).

433 Chlorite compositions are variable, though all of them have in common $\approx 50\%$ clinocllore
434 + daphnite and $\approx 50\%$ amesite + sudoite (Fig. 5b). Chlorites in sample PLB-88 are poor in
435 amesite with a large variation of clinocllore + daphnite and sudoite. In sample PLB-84
436 chlorites, variable compositions between amesite and sudoite indicate a variation of Al^{IV} ,
437 which implies an increase of temperature from rims to cores as shown in the chemical maps
438 of Fig. 4c. Finally, PLB-93 chlorites are poor in sudoite and higher in Al^{IV} content, thus
439 suggesting higher average temperatures- (Vidal et al., 2006). Altogether, chlorite
440 compositional data suggest the presence of two end-members: sudoite-rich low-temperature
441 (PLB-88), and amesite-rich high-temperature (PLB-93).

442 Maps of Al^{IV} in chlorites have been represented in Fig. 4c. Sample PLB-88 shows lower Al^{IV}
443 content ($\approx 1.1-1.3$ apfu) than sample PLB-93 ($\approx 1.3-1.5$ apfu). In sample PLB-84, some large
444 chlorite grains oriented along S_1 are zoned, with higher Al^{IV} content in the cores (≈ 1.4 apfu)
445 than in the rims (≈ 1.0 apfu; see white square in Fig. 4c). According to the empirical
446 calibration of Cathelineau (1988), Al^{IV} in chlorites increases with temperature. Thus, the Al^{IV}

447 content in chlorites manifests different temperatures in different samples, and also from core
448 to rim in singular grains.

449 Temperature maps have been obtained with the semi-empirical thermometer of Lanari et al.
450 (2014b), assuming that Fe^{2+} is the Fe total (Fig. 4d). Temperatures range between 100-200
451 °C in sample PLB-88, 150-350 °C in sample PLB-84, and 200-450 °C in sample PLB-93.
452 Tiny chlorites developed along S_2 show lower temperatures than larger and more abundant
453 chlorites along S_1 , with the exception of sample PLB-93. Furthermore, some large chlorites
454 oriented along S_1 are zoned, showing high-temperature relic cores (350-450 °C; see white
455 insets in Fig. 4c-d) surrounded by low-temperature rims (150-250 °C).

456 To test Vidal et al. (2005, 2006) and Bourdelle et al. (2013) approaches, an area of
457 representative chlorites in an S_1 microlithon was selected from each map (see red insets in
458 Fig. 4d). Corresponding chlorite compositions were extracted and introduced in the chlorite-
459 quartz-water equilibria (Fig. 7a, Vidal et al., 2005, 2006; Fig. 7b, Bourdelle et al., 2013). The
460 temperature estimates (Fig. 7) are fairly similar with both methods, averaging 120-230 °C in
461 sample PLB-88 and 150-380 °C in sample PLB-84. This is also in agreement with the
462 temperature maps calculated with the Lanari et al. (2014a) model. Only the sample PLB-93
463 shows a divergence on temperature averages: mostly ~~200~~150-250 °C with the thermometer
464 of Bourdelle et al. (2013), and 250-350 °C with the one of Vidal et al. (2005, 2006).
465 ~~Nevertheless, the Bourdelle thermometer predicts temperatures up to 380-400°C.~~ In both
466 cases, ~~(Bourdelle et al. (2013) and Vidal et al. (2005, 2006) approaches)~~, the higher
467 temperature analyses are obtained from crystal cores and belong mostly to the sample PLB-
468 93.

469

470 4.3. RSCM thermometry

471 The ratio parameters and corresponding maximum temperatures obtained from all the
472 spectra analyzed are shown in the supplementary information. The Raman spectra were
473 decomposed into bands following the appropriate fitting procedure described in Beyssac et
474 al. (2002a) for the lower formations (high-temperature Raman spectra; ratio parameter R2)
475 and Lahfid et al. (2010) for the Santa Iria formation (low-temperature Raman spectra; ratio
476 parameters RA1 and RA2; Fig. 3). The average temperatures are shown in Table 1 and Fig.
477 1c with a relative colour bar from red (higher temperature) to blue (lower temperature). The
478 average temperatures for the lower formations range from 420 to 530 °C, with a mean value
479 of 468 °C (standard deviation of 35). The highest temperatures are found in samples PLB-
480 82 (530 °C) and PLB-93 (495 °C), while the remaining ones do not exceed 480 °C. As for
481 the Santa Iria formation, temperatures are lower (315-330 °C; Table 1) than in the underlying
482 formations.

483

484 5. Interpretation and discussion

485 5.1. Deformation/metamorphism relationships

486 The obtained analytical results must be interpreted in the context of the Variscan evolution of
487 the Pulo do Lobo ~~beltdomain~~. As described above, two regional deformational events D_1

488 and D₂ gave way to the development of foliations (Devonian S₁ and Carboniferous S₂)
489 accompanied by metamorphic phyllosilicate growth (M₁ and M₂). In the cross-sections of
490 Fig. 1c, KI values derived from XRD and average temperature from RSCM ~~are represented.~~
491 ~~The suggest that the~~ lowest metamorphic grade (green and blue colours) corresponds to the
492 Santa Iria formation. ~~Moreover, Table 2 summarizes the relationship between deformation~~
493 ~~and metamorphism of the Pulo do Lobo belt in the context of the Variscan tectonic~~
494 ~~evolution of SW Iberia (Pérez-Cáceres et al., 2015).~~

495 The textural observations evidence that in most samples of the lower formations M₁ was the
496 main crystallization event, developing abundant and large-sized white mica and chlorite in S₁
497 microlithons, while M₂ gave way to small-sized white mica (e.g., Fig. 2e and map 1 in Fig. 4).
498 On the other hand, polydeformed rocks commonly show previously grown minerals rotated
499 towards a new foliation developed at lower-grade conditions, without new crystallization.
500 This can be the case of the white micas that define S₂ in some samples (illustrated in Fig. 2d),
501 which, in turn, is not contradictory with the similar chemical composition of S₁ and S₂ micas
502 (Fig. 5a). As shown in ~~our~~ these samples, S₁ is variably crenulated by D₂, so that M₁ minerals
503 are variably rotated towards S₂. Consequently, the metamorphic data obtained from the
504 samples of the lower formations will be ascribed to D₁-M₁. Sample PLB-93 might represent
505 an exception, since its slightly higher RSCM and chlorite-derived temperatures might be due
506 to nearby intrusions (Fig. 1b and 1c.1). At this respect, it is important to note the
507 Mississippian transtensional event (basins development and abundant mafic magmatism)
508 that took place between D₁ and D₂ (Pérez-Cáceres et al., 2015). The characterization of M₂
509 can be done by studying the samples from the Santa Iria formation, which are only affected
510 by S₂ accompanied by small-sized phyllosilicate growth (Fig. 2f). No crystallization has been
511 observed related to the S3 disjunctive crenulation cleavage.

512

513 5.2. First tectonothermal event (Devonian M₁)

514 The observed mineral association (Qz + Ab + Ms + Chl ± Pg), together with the presence
515 of C/S is compatible with low-grade metamorphic conditions (Table 1). White mica
516 “crystallinity” values (0.17-0.22 Δ°2θ; average 0.19) are always in the range of the epizone
517 (low-grade or greenschists facies; >300 °C; Frey, 1987; Kisch, 1987, Warr and Ferreiro
518 Mähnlmann, 2015), in accordance with the values reported by Abad et al. (2001) in a more
519 general study of the diagenetic-metamorphic evolution of the South Portuguese Zone
520 metapelites. Nevertheless, both the values of KI, still far from 0.14 Δ°2θ, (high epizone
521 conditions according to Abad et al., 2006), and their variability, suggest that temperature was
522 not high enough as to stabilize a highly crystalline white mica ~~at high epizone conditions~~
523 ~~(Abad et al., 2006).~~ This is in agreement with the low Na content of K-micas coexisting with
524 paragonite (Fig. 6), meaning a very-low temperature position in the muscovite-paragonite
525 solvus for natural quasi-binary Pg-Ms pairs (Guidotti et al., 1994). By contrast, the maximum
526 temperatures obtained with RSCM geothermometry are surprisingly high (420-530 °C;
527 average 470 °C; corresponding to very high epizone or even medium-grade conditions; Table
528 1).

529 The composition of paired chlorite and white mica is normally used to calculate pressure and
530 temperature (e.g., Vidal et al., 2006), but multi-equilibrium approach was not successful

531 because the P-T equilibrium conditions did not converge. This result is indicative of chemical
532 disequilibrium, precluding their use as a reliable geothermobarometer in this case. The
533 temperatures calculated from chlorite compositions following various approaches (Vidal et
534 al., 2006, Fig. 7a; Bourdelle et al., 2013, Fig. 7b; Lanari et al., 2014a, Fig. 4d) are as follow:
535 ~~120-100~~-230 °C for sample PLB-88, ~~150-380~~~~375~~ °C for sample PLB-84, and ~~250-400~~~~150-450~~
536 °C for sample PLB-93 ~~and a small population of chlorite cores from sample PLB-84~~ (Figs.
537 ~~4d~~ and 7, and Table 1). The slightly higher temperature of sample PLB-93 is inferred from
538 its highest white mica “crystallinity” (0.17 $\Delta^{\circ}2\theta$), high RSCM temperature (495 °C), high-
539 temperature (amesite-rich) chlorite and higher chlorite thermometry (Table 1), and can be
540 explained by its nearness to metric-scale mafic igneous bodies of the Peramora Mélange
541 (located at \approx 200 m to the south; Pérez-Cáceres et al., 2015) and/or to a granite stock (located
542 at \approx 5 km to the west) (Fig. 1b).

543 In our samples there is some evidence of chlorite retrogression: (i) the chemical
544 disequilibrium showed by the white mica/chlorite geothermobarometer, (ii) the presence of
545 C/S mixed layers not stable in the epizone (e.g. Potel et al., 2006), (iii) the difference between
546 temperature estimates from crystal rims to cores, and the higher temperature relic cores
547 preserved in large chlorites defining S_1 (Fig. 4c-d), and (iv) the previously reported XRD and
548 TEM data of chlorite retrograded to smectite and corrensite in the Pulo do Lobo ~~belt domain~~
549 (see fig. 1 in Nieto et al., 2005). The existence of chlorites with different compositions
550 crystallized at different temperatures is the usual scenario (e.g., Vidal et al., 2006, 2016; Lanari
551 et al., 2012; 2014a and b; Grosch et al., 2012; 2014; Cantarero et al., 2014). In such situation,
552 the definition of a single temperature and pressure attributable to peak conditions is really
553 difficult. The maximum temperature showed by chlorite relic cores is 350-450 °C (Fig. 4d),
554 which is more in accordance with the conditions estimated for M_1 by means of ~~white mica~~
555 “crystallinity” and RSCM data.

556 An issue that deserves some discussion is the difference in temperature estimates between
557 RSCM and other techniques. RSCM thermometry records the peak temperature and is not
558 sensitive to the retrograde path. Alternatively, other methods based on phyllosilicate
559 compositions are prone to record reequilibration during the retrograde path; thus, they rarely
560 record the peak conditions, except perhaps in the core of certain large crystals. Therefore,
561 RSCM and phyllosilicate-based methods do not record the same information on
562 temperature, being in fact complementary. The analyzed CM grains were carefully
563 checked by microtextural observation and spectral geometry to make sure that these grains
564 are actually derived from in situ organic matter graphitized during metamorphism.

565 In our case study, at the high peak temperature given by the RSCM thermometry, minerals
566 such as biotite or garnet are expected to crystallize in metasediments, though they have not
567 been observed in our samples. The absence of such minerals Biotite has been said to exist in
568 a few previous works (Apalategui et al., 1983; Braid et al., 2010; Rubio Pascual et al., 2013).
569 However, in a few of our samples, biotite-looking crystals have resulted to be oxichlorites
570 under SEM analyses. The absence or exceptional presence of biotite can be due to whole-
571 rock composition, and explained by growth inhibition related to Na-excess, as evidenced by
572 the presence of albite and paragonite in our samples. Another possible explanation could be
573 the higher sensitivity of CM graphitization to fast reequilibration during a short-time thermal
574 event. Thus, the Mississippian intrusions subsequent to M_1 in the Pulo do Lobo formation

575 (see description in section 2) could have exerted a fast and locally intense thermal imprint
576 that influenced CM but not the crystal chemistry of silicates. Moreover, recrystallization
577 processes are not only function of temperature, but also promoted by deformation/stress,
578 time, fluid/rock ratio (Merriman and Frey, 1999). Observations of this kind (differing
579 reaction kinetics between organic and inorganic material (e.g. illite) in a contact metamorphic
580 setting can be found in Olsson (1999) and Abad et al. (2014). Regarding the time of geological
581 processes, Mori et al. (2017) investigated the importance of heating duration for RSCM
582 thermometry by studying graphitization around dykes. They showed that small-scale
583 intrusions generating short thermal events modify the structure of CM in the surrounding
584 rocks, to conclude that CM crystallinity is clearly related to contact metamorphism. The
585 influence of low-pressure contact aureoles on RSCM temperature patterns is further
586 supported by the results obtained by Hilchie and Jamieson (2014), who concluded that the
587 variation of RSCM temperatures can be controlled by the subsurface geometry of a pluton.
588 Finally, the long-distance thermal influence of plutonic intrusions on low-grade rocks located
589 as far as 10 km has already been evidenced (e.g., Merriman and Frey, 1999; Martínez Poyatos
590 et al., 2001) and could also be recorded by RSCM thermometry in our samples.

591

592 5.3. Second tectonothermal event (middle/upper Carboniferous M₂)

593 The mineralogy of the Santa Iría samples (Qz + Fsp + Ms + Chl ± C/S) is compatible with
594 very low- to low-grade conditions. The K-white mica “crystallinity” values (0.20-0.26 Δ°2θ;
595 average 0.23) point to lower epizone conditions, very close to the boundary with the
596 anchizone (≈300 °C; Frey, 1987; Kisch, 1987). The temperatures calculated by RSCM in two
597 samples (315 and 330 °C) are compatible with the KI data of XRD analysis.

598 Our metamorphic data corroborate the existence of an unconformity between the lower and
599 upper formations of the Pulo do Lobo ~~belt~~ (Pérez-Cáceres et al., domain (Pérez-Cáceres et
600 al., 2015). Table 2 summarizes the relationship between deformation and metamorphism of
601 the Pulo do Lobo domain in the context of the Variscan tectonic evolution of SW Iberia
602 (Pérez-Cáceres et al., 2015). The lower formations record a Devonian tectonothermal event
603 that reached epizone or lower greenschist facies conditions (M₁ with generalized
604 phyllosilicate growth at temperatures as high as 450 °C), while the overlying upper formation
605 records a middle/upper Carboniferous tectonothermal event close to the anchizone/epizone
606 boundary (M₂ with small-sized phyllosilicate growth at temperatures ≈300-330 °C; Table 1).
607 Obviously, M₂ also affected somehow the lower formations, being, at least in part, the
608 responsible for the observed retrogression of M₁ chlorite and/or crystallization of new
609 chlorites at lower temperature.

610

611 5.4. Pressure conditions

612 The measured *b*-cell parameters of K-white mica (in a short range between 8.991-9.002 Å;
613 average 8.996; standard deviation 0.003) are very similar in the lower and upper formations
614 of the Pulo do Lobo ~~belt~~ domain. Thus, the *b* parameter is consistently homogeneous and
615 reflects very low phengite substitution in mica, as expected at low-pressure settings (Potel et
616 al., 2006, 2016), near the intermediate pressure gradient boundary (Guidotti and Sassi, 1986).

617 In agreement with the low *b*-cell parameters, the composition of K-white mica is close to
618 muscovite with very low celadonite and higher pyrophyllite content (Fig. 5a), as expected for
619 illite-rich mica formed at low-pressure gradients. In the case of high- or medium-pressure
620 conditions, a continuous trend in mica compositions would be found reflecting the
621 decompression path after the peak pressure, while the *b*-cell parameter would represent an
622 average value of the range of mica compositions found in the sample (Abad et al., 2003b).
623 On the contrary, at low-pressure settings, the overall range of recorded pressure is very short
624 and micas present similar compositions and *b*-cell parameters among the various samples, as
625 in the case of the Pulo do Lobo samples (Figs. 5a and 6, and Table 1).

626 The Pulo do Lobo ~~belt~~domain has been classically interpreted as a pre-collisional subduction-
627 related accretionary prism, based on the MORB geochemistry of their mafic rocks (see
628 section 2.1). According to this classical interpretation, features typical of modern subduction
629 systems should be expected, such as high-pressure metamorphic gradient remnants of partial
630 subduction/exhumation in an accretionary wedge (e.g., Platt, 1986; Ernst, 2005), or slices of
631 oceanic slab-derived lithologies (varied mid-ocean ridge metaigneous lithologies and also
632 deep ocean bottom metasediments). Thus, recent works on the Makran accretionary prism
633 (Omran et al., 2017) and the subduction system of Japan (Endo and Wallis, 2017) describe
634 an accretionary mélange complex composed of pelagic sedimentary rocks, ophiolites,
635 greenschists, amphibolites, and blueschists with high-pressure minerals such as lawsonite and
636 glaucophane. On the contrary, most of the geological data concerning the Pulo do Lobo
637 ~~belt~~domain do not back up such interpretation (see section 2.1), and our new results about
638 pressure conditions are also in disagreement. The only suspect of high-pressure gradient in
639 the Pulo do Lobo ~~belt~~domain is the interpretation of some rhomboidal aggregates of
640 epidote porphyroblasts as the remnants of supposed lawsonite grown previously to S₂ in some
641 samples of Pulo do Lobo mafic schists (Rubio Pascual et al., 2013). However, no analytical
642 data have been presented to support the lawsonite pseudomorphs.

643

644 6. Conclusions

645 Eighteen samples of metapelites from the Pulo do Lobo ~~belt~~domain have been studied to
646 characterize their Variscan low-grade metamorphism. The microstructural analysis of the
647 samples of the lower formations (Devonian Pulo do Lobo and Ribeira de Limas) shows the
648 existence of two superposed low-grade tectonothermal events with associated foliation and
649 phyllosilicate growth (S₁-M₁ and S₂-M₂; Table 2). M₂ was less intense, being the only event
650 that affected the overlying Carboniferous Santa Iria formation. The regional geology also
651 shows that a Mississippian thermal (magmatic-derived) event occurred in-between M₁ and
652 M₂.

653 M₁ and M₂ correspond to the chlorite zone, but M₁ entered the epizone (greenschists facies
654 with temperatures up to ≈450 °C), while M₂ did not exceed the anchizone-epizone boundary
655 (≈300 °C).

656 The temperatures obtained from RSCM are higher compared to the ones derived from
657 chlorite geothermometry and white mica data. The discrepancy can be explained by the fact
658 that RSCM records the true maximum temperature, being not affected by retrogression as

659 other methods do. In addition, this difference can be the consequence of the high sensitivity
660 of CM to quickly equilibrate at maximum temperatures during short thermal events due to
661 magmatic intrusions emplaced during the Mississippian thermal event.

662 Thermodynamic disequilibrium between white mica and chlorite has precluded their use for
663 geothermobarometry, and a variety of data (including the existence of relic high-temperature
664 chlorite cores, the presence of chlorite/smectite mixed layers, or the very-low temperatures
665 calculated with chlorite geothermometers) indicate chlorite retrogression after M₁
666 metamorphic climax and crystallization of new chlorite grains at lower temperature.

667 The low-pressure conditions derived from white mica indicators (very low celadonite content
668 and *b*-cell values) are incompatible with the high-pressure metamorphic gradient expected in
669 a subduction-related accretionary wedge, which has been the classical interpretation of the
670 Pulo do Lobo [belt domain](#).

671

672

673 Acknowledgements

674 This work was supported by the projects CGL2011-24101 (Spanish Ministry of Science and
675 Innovation), CGL2015-71692-P and CGL2016-75679-P (Spanish Ministry of Economy and
676 Competitiveness), RNM-148 and RNM-179 (Andalusian Government) and BES-2012-
677 055754 (Doctoral scholarship to I. Pérez-Cáceres from the Spanish Ministry of Science and
678 Innovation). The Raman facility in Paris has been funded by the City of Paris (Emergence
679 program). We thank Valérie Magnin for her assistance with the microprobe analysis in
680 Grenoble and Pierre Lanari for his support with thermodynamic software. [Detailed revisions](#)
681 [by C. Quesada and an anonymous reviewer contributed to improve this paper.](#)

682

683 Figure captions

684 **Figure 1.** a) Location of the studied area in the SW of the Iberian Massif (in grey). CIZ: Central
685 Iberian Zone, OMZ: Ossa-Morena Zone, SPZ: South Portuguese Zone. b) Geological map of the
686 Pulo do Lobo [belt domain](#) and other units related to the OMZ/SPZ boundary with indications of the
687 two cross-sections studied: [and collected samples](#). c.1-2) Geological cross-sections of the Pulo do
688 Lobo [belt domain](#) (see b for location) (modified from Martínez Poza et al., 2012 and Pérez-Cáceres
689 et al., 2015). Numbered red circles in b-c locate the samples studied. Big circles show the KI values
690 for 10 Å reflection peaks of K-white mica and the average RSCM temperatures, with the relative
691 colour bar according to the results shown in Table 1. BAA: Beja-Acebuches Amphibolites, M:
692 metabasalts, PL: Pulo do Lobo formation, RL: Ribeira de Limas formation, SI: Santa Iria formation.

693 **Figure 2.** Pictures of the Pulo do Lobo rocks illustrating deformation at outcrop scale: a) Pulo do
694 Lobo formation, b) Ribeira de Limas formation, c) Santa Iria formation. Microphotographs from
695 thin-sections: d) Cross-polarized light image of sample PLB-84 (Pulo do Lobo formation), e) SEM-
696 BSE image of sample PLB-88 (Ribeira de Limas formation), f) Cross-polarized light images of sample
697 PLB-71 (Santa Iria formation).

698 **Figure 3.** Representative Raman spectra of CM across the Pulo do Lobo [belt domain](#) from low
699 temperature (bottom; Santa Iria formation) to high temperature (top; lower formations) including the

700 average maximum temperatures (°C) for each sample. Vertical scale for spectrum intensity is arbitrary.
701 See Fig. 1 for sample location and Table 1 and supplementary information for RSCM data.

702 **Figure 4.** X-Ray maps of the three selected samples analyzed by EPMA and processed with
703 XMapTools. The samples belong to the lower formations of the Pulo do Lobo ~~belt~~domain (sample
704 PLB-88: Ribeira de Limas formation; samples PLB-84 and PLB-93: Pulo do Lobo formation; the
705 latter (PLB-93) is close to Early Carboniferous igneous intrusions). a) EPMA BSE photographs. b)
706 Mineral maps. c) Al^{IV} content map in chlorites, which increases with temperature. The white square
707 highlights the zonation of a chlorite grain from core to rim. d) Temperature maps of chlorite using
708 the Lanari et al. (2014a) geothermometer assuming all iron as ferrous. White squares show selected
709 areas illustrating higher-temperature chlorite cores. Red squares show the selected areas
710 (representative of S₁ foliation) used for chlorite-quartz-water geothermometric calculations shown in
711 Fig. 7.

712 **Figure 5.** Ternary plots of all the analyzed white micas (a) (Cel: celadonite, Mus: muscovite, Prl:
713 pyrophyllite) and chlorite (b) (Cli+Daph: clinocllore + daphnite, Am: amesite, Sud: sudoite) plotted
714 with the XmapTools TriPlot3D module. Colour bars refer to the number of mica/chlorite pixels
715 analyzed.

716 **Figure 6.** Compositional diagram of white micas showing Na/(Na+K) vs Si/Al (atomic ratios) for 31
717 EPMA point analyses from seven samples of the lower formations of the Pulo do Lobo ~~belt~~domain
718 (different symbology, for each sample). Point analyses were obtained on the microprobe at the
719 University of Huelva (Spain). Qualitative information about temperature and pressure conditions are
720 respectively according to Guidotti et al. (1994), Coggon and Holland (2002), Parra et al. (2002),
721 Massonne and Schereyer (1987) and Massonne and Szpurka (1997).

722 **Figure 7.** Histograms of temperatures obtained using the chlorite-quartz-water geothermometer of
723 Vidal et al. (2006) (a) and Bourdelle et al. (2013) (b) on selected representative S₁ chlorites (see red
724 squares in Fig. 4d for location). *n* represents the number of chlorites that could be used for each
725 calibration. The number of analyses is lower in those with Vidal et al. (2006) approach because the
726 assumption that the Si content of chlorite is lower than 3 apfu.

727

728

729 Table captions

730 **Table 1.** Samples and results obtained by XRD (<2 μm fraction), white mica and chlorite
731 compositions, temperature ranges from chlorite thermometry, and average RSCM thermometry.
732 ~~Basel~~ KI values and average RSCM temperatures show a relative colour-bar scale. Mineral
733 abbreviations according to Whitney & Evans (2010). Qz: Quartz, Ms: Muscovite, Fsp:
734 ~~Feldspar~~Feldspar, Chl: Chlorite, Pg: paragonite, C/S: chlorite-smectite mixed layers, Cel: celadonite,
735 Prl: pyrophyllite, Cli+Daph: clinocllore + daphnite, Am: amesite, Sud: sudoite, Std Dv: standard
736 deviation.

737 **Table 2.** Summary of the tectonometamorphic Variscan evolution of the Pulo do Lobo
738 ~~belt~~domain.

739

740

741 References

- 742 Abad, I., Mata, M.P., Nieto, F., and Velilla, N.: The phyllosilicates in diagenetic-metamorphic rocks
743 of the South Portuguese Zone, southwestern Portugal, *The Canadian Mineralogist*, 39(6),
744 1571-1589, 2001.
- 745 Abad, I., Nieto, F., and Velilla, N.: Chemical and textural characterisation of diagenetic to low-grade
746 metamorphic phyllosilicates in turbidite sandstones of the South Portuguese Zone: A
747 comparison between metapelites and sandstones, *Schweizerische Mineralogische und*
748 *Petrographische Mitteilungen*, 82(2), 303-324. 2002.
- 749 Abad, I., Nieto, F., and Gutiérrez-Alonso, G.: Textural and chemical changes in slate-forming
750 phyllosilicates across the external-internal zones transition in the low-grade metamorphic
751 belt of the NW Iberian Variscan Chain, *Swiss Bulletin of Mineralogy and Petrology*, 83(1),
752 63-80, 2003a.
- 753 Abad, I., Gutierrez-Alonso, G., Nieto, F., Gertner, I., Becker, A., and Cabero, A.: The structure and
754 the phyllosilicates (chemistry, crystallinity and texture) of Talas Ala-Tau (Tien Shan, Kyrgyz
755 Republic); comparison with more recent subduction complexes, *Tectonophysics*, 365(1-4),
756 103-127, 2003b.
- 757 Abad, I., Nieto, F., Gutiérrez-Alonso, G., Campo, M. D., López-Munguira, A., and Velilla, N.: Illitic
758 substitution in micas of very low-grade metamorphic clastic rocks. *European Journal of*
759 *Mineralogy*, 18(1), 59-69, 2006.
- 760 Abad, I., Nieto, F., Velilla, N., and Suárez-Ruiz, I.: Metamorphic evidences from the Monchique
761 pluton (South Portugal): Contact metamorphism vs regional metamorphism under very low-
762 grade conditions, *Revista de la Sociedad Geológica de España*, 27(1): 337-350, 2014.
- 763 Abalos, B., Gil Iburguchi, J.I., and Eguiluz, L.: Cadomian subduction/collision and Variscan
764 transpression in the Badajoz-Córdoba shear belt, southwest Spain, *Tectonophysics*, 199, 51-
765 72, 1991.
- 766 Airaghi, L., Lanari, P., de Sigoyer, J., and Guillot, S.: Microstructural vs compositional preservation
767 and pseudomorphic replacement of muscovite in deformed metapelites from the Longmen
768 Shan (Sichuan, China), *Lithos*, 282, 262-280, 2017.
- 769 Ali, A.: The tectono-metamorphic evolution of the Balcooma Metamorphic Group, north-eastern
770 Australia: a multidisciplinary approach, *Journal of Metamorphic Geology*, 28(4), 397-422,
771 2010.
- 772 Apalategui, O., Barranco, E., Contreras, F., Delgado, M., and Roldán, F. J.: Hoja 916, Aroche, Mapa
773 Geológico de España a escala 1:50000, Inst. Geológico y Minero de España, Madrid, 1983.
- 774 Araújo, A., Fonseca, P., Munhá, J., Moita, P., Pedro, J., and Ribeiro, A.: The Moura Phyllonitic
775 Complex: an accretionary complex related with obduction in the southern Iberia Variscan
776 suture, *Geodinamica Acta*, 18, 375-388, 2005.
- 777 Arenas, R., Abati, J., Martínez Catalán, J.R., García, F. D., and Pascual, F.R.: PT evolution of eclogites
778 from the Agualada Unit (Ordenes Complex, northwest Iberian Massif, Spain): Implications
779 for crustal subduction, *Lithos*, 40(2), 221-242, 1997.
- 780 Azor, A., González Lodeiro, F., and Simancas, J.F.: Tectonic evolution of the boundary between the
781 Central Iberian and Ossa-Morena zones (Variscan Belt, southwest Spain), *Tectonics*, 13, 45-
782 61, 1994.
- 783 Azor, A., Rubatto, D., Simancas, J.F., González Lodeiro, F., Martínez Poyatos, D., Martín Parra L.M.,
784 and Matas, J.: Rheic Ocean ophiolitic remnants in Southern Iberia questioned by SHRIMP
785 U-Pb zircon ages on the Beja-Acebuches amphibolites, *Tectonics*, 27(5), 2008.

Con formato: Inglés (Estados Unidos)

Con formato: Inglés (Reino Unido)

Con formato: Inglés (Reino Unido)

- 786 Azor, A., Simancas, J.F., Martínez Poyatos, D., Pérez-Cáceres, I., González Lodeiro, F., and Expósito,
787 I.: Chapter 10.3: Deformation and Structure, Southwestern Iberia, in: *The Geology of Iberia:*
788 *A Geodynamic Approach, Volume 2: The Variscan Cycle*, edited by: Quesada, C., and
789 Oliveira, J.T., Springer, 316-335, 2019.
- 790 Barbero, L.: Granulite-facies metamorphism in the Anatectic Complex of Toledo, Spain: late
791 Hercynian tectonic evolution by crustal extension, *Journal of the Geological Society*, 152(2),
792 365-382, 1995.
- 793 Bard, J.P. : Signification tectonique des métatholeites d'anité abyssale de la ceinture de base pression
794 d'Aracena (Huelva, Espagne), *Bulletin de la Société Géologique de France*, 19, 385-393,
795 1977.
- 796 Bastida, F., Martínez-Catalán, J.R., and Pulgar, J.A.: Structural, metamorphic and magmatic history
797 of the Mondoñedo nappe (Hercynian belt, NW Spain). *Journal of Structural Geology*, 8(3-
798 4), 415-430, 1986.
- 799 Bastida, F., Brime, C., García-López, S. Aller, J., Valin, M.L., and Sanz-López, J.: Tectono-thermal
800 evolution of the Cantabrian Zone (NW Spain), in: *Palaeozoic conodonts from northern*
801 *Spain*, edited by: García López, S., and Bastida, F., Instituto Geológico y Minero de España,
802 Cuadernos del Museo Geominero, 1, 105-123, Madrid, ISBN: 84-7840-446-5, 2002.
- 803 Battaglia, S., Leoni, L., and Sartori, F.: The Kübler index in late diagenetic to low-grade metamorphic
804 pelites: a critical comparison of data from 10 Å and 5 Å peaks, *Clays and Clay Minerals*,
805 52(1), 85-105, 2004.
- 806 Beyssac, O., Goffé, B., Chopin, C., and Rouzaud, J.N.: Raman spectra of carbonaceous material in
807 metasediments: a new geothermometer, *Journal of Metamorphic Geology*, 20, 859-871,
808 2002a.
- 809 Beyssac, O., Rouzaud, J.-N., Goffé, B., Brunet, F., and Chopin, C.: Graphitization in a high-pressure,
810 low temperature metamorphic gradient: a Raman microspectroscopy and HRTEM study.
811 *Contrib. Mineral. Petrol.*, 143, 19-31, 2002b.
- 812 Beyssac, O., Goffé, B., Petitot, J.P., Froigneux, E., and Rouzaud, J.N.: On the characterization of
813 disordered and heterogeneous carbonaceous materials using Raman spectroscopy,
814 *Spectrochim. Acta A Mol. Biomol. Spectrosc.*, 59, 2267-2276, 2003.
- 815 Beyssac, O., Bollinger, L., Avouac, J.P., and Goffé, B.: Thermal metamorphism in the lesser Himalaya
816 of Nepal determined from Raman spectroscopy of carbonaceous material, *Earth and*
817 *Planetary Science Letters*, 225, 233-241, 2004.
- 818 Booth-Rea, G., Simancas, J.F., Azor, A., Azañón, J.M., Gonzalez Lodeiro, F., and Fonseca, P.: HP-
819 LT Variscan metamorphism in the Cubito-Moura schists (Ossa-Morena Zone, southern
820 Iberia), *Comptes Rendus Geoscience*, 338(16), 1260-1267, 2006.
- 821 Bourdelle, F., Parra, T., Chopin, C., and Beyssac, O.: A new chlorite geothermometer for diagenetic
822 to low-grade metamorphic conditions, *Contributions to Mineralogy and Petrology*, 165(4),
823 723-735, 2013.
- 824 Bousquet, R., Oberha, R., Goffé, B., Wiederkehr, M., Koller, F., Schmid, S.M., Schuster, R., Engi,
825 M., Berger, A., and Martinotti, G.: Metamorphism of metasediments at the scale of an
826 orogen: a key to the tertiary geodynamic evolution of the Alps, *Geological Society, London,*
827 *Special Publications*, 298, 393-411, 2008.

- 828 Braid, J.A., Murphy, J.B., and Quesada, C.: Structural analysis of an accretionary prism in a continental
829 collisional setting, the Late Paleozoic Pulo do Lobo Zone, Southern Iberia, *Gondwana*
830 *Research*, 17(2-3), 422-439, 2010.
- 831 Braid, J. A., Murphy, J. B., Quesada, C., and Mortensen, J.: Tectonic escape of a crustal fragment
832 during the closure of the Rheic Ocean: U–Pb detrital zircon data from the Late Palaeozoic
833 Pulo do Lobo and South Portuguese zones, southern Iberia, *Journal of the Geological*
834 *Society*, 168(2), 383-392, 2011.
- 835 [Braid, J. A., Murphy, J. B., Quesada, C., Gladney, E. R. and Dupuis, N.: Progressive magmatism and](#)
836 [evolution of the Variscan suture in southern Iberia. *International Journal of Earth Sciences*,](#)
837 [107\(3\), 971-983, 2018.](#)
- 838 Brown, M.: P–T–t evolution of orogenic belts and the causes of regional metamorphism, *Journal of*
839 *the Geological Society*, 150(2), 227-241, 1993.
- 840 Burg, J.P., Iglesias, M., Laurent, P., Matte, P., and Ribeiro, A.: Variscan intracontinental deformation:
841 the Coimbra–Córdoba Shear zone (SW Iberian Peninsula), *Tectonophysics*, 78, 161-177,
842 1981.
- 843 Cantarero, I., Lanari, P., Vidal, O., Alías, G., Travé, A., and Baqués, V.: Long-term fluid circulation
844 in extensional faults in the central Catalan Coastal Ranges: P–T constraints from neoformed
845 chlorite and K-white mica, *International Journal of Earth Sciences*, 103(1), 165-188, 2014.
- 846 Castro, A., Fernández, C., De la Rosa, J.D., Moreno Ventas, I., and Rogers, G.: Significance of
847 MORB-derived amphibolites from the Aracena metamorphic belt, southwest Spain, *Journal*
848 *of Petrology*, 37(2), 235-260, 1996.
- 849 Castro, A., Fernández, C., El-Hmidi, H., El-Biad, M., Díaz, M., De la Rosa, J., and Stuart, F.: Age
850 constraints to the relationships between magmatism, metamorphism and tectonism in the
851 Aracena metamorphic belt, southern Spain, *International Journal of Earth Sciences*, 88(1),
852 26-37, 1999.
- 853 Cathelineau, M.: Cation site occupancy in chlorites and illites as a function of temperature, *Clay*
854 *Minerals* 23, 471-485, 1988.
- 855 Cathelineau, M., and Nieva, D.: A chlorite solid solution geothermometer the Los Azufres (Mexico)
856 geothermal system, *Contrib. Mineral Petrol.*, 91(3), 235-244, 1985.
- 857 Coggon, R., and Holland, T.J.B.: Mixing properties of phengitic micas and revised garnet-phengite
858 thermobarometers, *Journal of Metamorphic Geology*, 20(7), 683-696, 2002.
- 859 [Crespo-Blanc, A., and Orozco, M.: The Southern Iberian Shear Zone: a major boundary in the](#)
860 [Hercynian folded belt. *Tectonophysics*, 148\(3-4\), 221-227, 1988.](#)
- 861 [Crespo-Blanc, A.:](#) Evolución geotectónica del contacto entre la zona de Ossa-Morena y la zona
862 Surportuguesa en las sierras de Aracena y Aroche (Macizo Ibérico Meridional): Un contacto
863 mayor en la cadena Hercínica Europea, Ph.D. Thesis, Univ. de Granada, 327 pp., 1991.
- 864 Crouzet, C., Dunkl, I., Paudel, L., Arkai, P., Rainer, T.M., Balogh, K., and Appel, E.: Temperature
865 and age constraints on the metamorphism of the Tethyan Himalaya in Central Nepal: A
866 multidisciplinary approach, *Journal of Asian Earth Sciences*, 30(1), 113-130, 2007.
- 867 Dahn, D.R.L., Braid, J.A., Murphy, J.B., Quesada, C., Dupuis, N., and McFarlane C.R.M.:
868 Geochemistry of the Peramora Melange and Pulo do Lobo schist: Geochemical investigation
869 and tectonic interpretation of mafic melange in the Pangean suture zone, Southern Iberia,
870 *International Journal of Earth Sciences*, 103(5), 1415-1431, 2014.

Con formato: Inglés (Reino Unido)

Con formato: Inglés (Estados Unidos)

Con formato: Inglés (Reino Unido)

- 871 Dallmeyer, R.D., Fonseca, P.E., Quesada, C., and Ribeiro, A.: $^{40}\text{Ar}/^{39}\text{Ar}$ mineral age constraints for
872 the tectonothermal evolution of a variscan suture in Southwest Iberia, *Tectonophysics*, 222,
873 177-194, 1993.
- 874 De Andrade, V., Vidal, O., Lewin, E., O'Brien, P., and Agard, P.: Quantification of electron
875 microprobe compositional maps of rock thin sections: an optimized method and examples,
876 *Journal of Metamorphic Geology*, 24(7), 655-668, 2006.
- 877 Díaz Azpiroz, M., Fernández, C., Castro, A., and El-Biad, M.: Tectonometamorphic evolution of the
878 Aracena metamorphic belt (SW Spain) resulting from ridge-trench interaction during
879 Variscan plate convergence, *Tectonics*, 25(1), 2006.
- 880 Eden, C.P.: Tectonostratigraphic analysis of the northern extent of the oceanic exotic terrane,
881 Northwestern Huelva Province, Spain, Ph. D. Thesis, Univ. of Southampton, 214 pp., 1991.
- 882 Eden, C., and Andrews, J.: Middle to upper Devonian melanges in SW Spain and their relationship
883 to the Meneage formation in south Cornwall. *Proc. Ussher Soc.*, 7, 217-222, 1990.
- 884 Endo, S., and Wallis, S.R.: Structural architecture and low-grade metamorphism of the Mikabu-
885 Northern Chichibu accretionary wedge, SW Japan, *Journal of Metamorphic Geology*, 35(6),
886 695-716, 2017.
- 887 Ernst, W.G.: Tectonic history of subduction zones inferred from retrograde blueschist PT paths,
888 *Geology* 16(12), 1081-1084, 1988.
- 889 Ernst, W.G.: Alpine and Pacific styles of Phanerozoic mountain building: subduction-zone
890 petrogenesis of continental crust, *Terra Nova*, 17(2), 165-188, 2005.
- 891 Escuder Viruete, J., Arenas, R., and Martínez Catalán, J.R.: Tectonothermal evolution associated with
892 Variscan crustal extension in the Tormes gneiss dome (NW Salamanca, Iberian Massif,
893 Spain), *Tectonophysics*, 238(1-4), 117-138, 1994.
- 894 Fonseca, P., and Ribeiro, A.: Tectonics of the Beja-Acebuches ophiolite - a major suture in the Iberian
895 variscan foldbelt, *Geol. Rundsch.*, 82, 440-447, 1993.
- 896 Fonseca, P., Munhá, J., Pedro, J., Rosas, F., Moita, P., Araujo, A., and Leal, N.: Variscan ophiolites
897 and high-pressure metamorphism in southern Iberia. *Ofioliti*, 24, 259-268, 1999.
- 898 Franceschelli, M., Leoni, L., Memmi, I., and Puxeddu, M.: Regional distribution of Al-silicates and
899 metamorphic zonation in the low-grade Verrucano metasediments from the Northern
900 Apennines, Italy, *Journal of Metamorphic Geology*, 4(3), 309-321, 1986.
- 901 Frey, M.: Very low-grade metamorphism of clastic sedimentary rocks, in: *Low temperature*
902 *metamorphism*, edited by: Frey, M., Blackie, Glasgow, 9-58, 1987.
- 903 Frey, M., and Robinson, D.: *Low-Grade Metamorphism*, 313 pp. Blackwell Science Ltd, Cambridge,
904 1999.
- 905 Gil Ibarra, J., Mendia, M., Girardeau, J., and Peucat, J.J.: Petrology of eclogites and clinopyroxene-
906 garnet metabasites from the Cabo Ortegal Complex (northwestern Spain), *Lithos*, 25(1-3),
907 133-162, 1990.
- 908 Goffé, B., and Velde, B.: Contrasted metamorphic evolutions in thrust cover units of the
909 Briançonnais zone (French Alps): A model for the conservation of HP-LT metamorphic
910 mineral assemblages, *Earth and Planetary Science Letters*, 68(2), 351-360, 1984.

- 911 Grosch, E.G., Vidal, O., Abu-Alam, T., and McLoughlin, N.: P–T constraints on the metamorphic
 912 evolution of the Paleoproterozoic Kromberg type-section, Barberton greenstone belt, South
 913 Africa, *Journal of Petrology*, 53(3), 513-545, 2012.
- 914 Grosch, E.G., McLoughlin, N., Lanari, P., Erambert, M., and Vidal, O.: Microscale mapping of
 915 alteration conditions and potential biosignatures in basaltic-ultramafic rocks on early Earth
 916 and beyond, *Astrobiology*, 14(3), 216-228, 2014.
- 917 Guidotti, C.V., and Sassi, F.P.: Classification and correlation of metamorphic facies series by means
 918 of muscovite b data from low-grade metapelites, *Neues Jahrbuch für Mineralogie-
 919 Abhandlungen*, 153, 363-380, 1986.
- 920 Guidotti, C. V., Mazzoli, C., Sassi, F. P., and Blencoe, J. G.: Compositional controls on the cell
 921 dimensions of 2M1 muscovite and paragonite, *European Journal of Mineralogy*, 4(2), 283-
 922 297, 1992.
- 923 Guidotti, C.V., Sassi, F.P., Blencoe, J.G., and Selverstone, J.: The paragonite–muscovite solvus: I. P-
 924 T-X limits derived from the Na – K compositions of natural, quasibinary paragonite-
 925 muscovite pairs, *Geoch. Cosmochim. Acta*, 58, 2269–2275, 1994.
- 926 Gutiérrez-Alonso, G., and Nieto, F.: White-mica 'crystallinity', finite strain and cleavage development
 927 across a large Variscan structure, NW Spain, *Journal of the Geological Society*, 153(2), 287-
 928 299, 1996.
- 929 Hilchie, L.J., and Jamieson, R.A.: Graphite thermometry in a low-pressure contact aureole, Halifax,
 930 Nova Scotia, *Lithos*, 208, 21-33, 2014.
- 931 Jarosewich, E.J., Nelen, J.A., and Norberg, J.A.: Reference samples for electron microprobe analysis:
 932 *Geostandards Newsletter*, 4, 43-47, 1980.
- 933 Kisch, H.J.: Correlation between indicators of very low-grade metamorphism. In: *Low temperature
 934 metamorphism*, edited by: Frey, M., Blackie, Glasgow, 227-300, 1987.
- 935 Kisch, H.J.: Illite crystallinity: recommendations on sample preparation, X-ray diffraction settings,
 936 and interlaboratory samples, *Journal of Metamorphic Geology*, 9, 665–670, 1991.
- 937 Kübler, B. : Evaluation quantitative du metamorphism par la cristallinite de l'illite. *Bull. Centres Rech.
 938 Pau-SNPA* 2, 385-397, 1968.
- 939 Lahfid, A., Beyssac, O., Deville, E., Negro, F., Chopin, C., and Goffé, B.: Evolution of the Raman
 940 spectrum of carbonaceous material in low-grade metasediments of the Glarus Alps
 941 (Switzerland), *Terra Nova*, 22, 354-360, 2010.
- 942 Lanari, P., Guillot, S., Schwartz, S., Vidal, O., Tricart, P., Riel, N., and Beyssac, O. : Diachronous
 943 evolution of the alpine continental subduction wedge: evidence from P-T estimates in the
 944 Briançonnais Zone houillère (France-Western Alps), *Journal of Geodynamics*, 56-57, 39-54,
 945 2012.
- 946 Lanari, P., Vidal, O., de Andrade, V., Dubacq, B., Lewin, E., Grosch, E.G., and Schwartz, S.:
 947 XMapTools: A MATLAB©-based program for electron microprobe X-Ray image
 948 processing and geothermobarometry, *Computers & Geosciences*, 62, 227-240, 2014a.
- 949 Lanari, P., Rolland, Y., Schwartz, S., Vidal, O., Guillot, S., Tricart, P., and Dumont, T.: P–T–t
 950 estimation of deformation in low-grade quartz-feldspar-bearing rocks using thermodynamic
 951 modelling and ⁴⁰Ar/³⁹Ar dating techniques: example of the Plan-de-Phasy shear zone unit
 952 (Briançonnais Zone, Western Alps), *Terra Nova*, 26(2), 130-138, 2014b.

- 953 Lopes, G., Pereira, Z., Fernandes, P., Wicander, R., Matos, J.X., Rosa, D., and Oliveira, J.T.: The
 954 significance of reworked palynomorphs (middle Cambrian to Tournaisian) in the Viséan
 955 Toca da Moura Complex (South Portugal). Implications for the geodynamic evolution of
 956 Ossa Morena Zone, *Rev. Palaeobot. Palynol.*, 200, 1-23, 2014.
- 957 López-Carmona, A., Pitra, P., and Abati, J.: Blueschist-facies metapelites from the Malpica-Tui Unit
 958 (NW Iberian Massif): phase equilibria modelling and H₂O and Fe₂O₃ influence in high-
 959 pressure assemblages, *Journal of Metamorphic Geology*, 31(3), 263-280, 2013.
- 960 López Munguira, A., Nieto, F., Pardo, E. S., and Velilla, N.: The composition of phyllosilicates in
 961 Precambrian, low-grade metamorphic, clastic rocks from the Southern Hesperian Massif
 962 (Spain) used as an indicator to metamorphic conditions, *Precambrian Research*, 53(3-4), 267-
 963 279, 1991.
- 964 López Sánchez-Vizcaíno, V., Gómez Pugnairé, M.T., Azor, A., and Fernández Soler, J.M.: Phase
 965 diagram sections applied to amphibolites: a case study from the Ossa-Morena/Central
 966 Iberian Variscan suture (Southwestern Iberian Massif), *Lithos*, 68, 1-21, 2003.
- 967 Martínez Catalán, J.R.: Estratigrafía y estructura del Domo de Lugo (Sector Oeste de la Zona
 968 Asturoccidental-leonesa), *Corpus Geol. Gallaeacae (2º Serie)*, 2, 1-291, 1985.
- 969 Martínez Catalán, J.R., Rubio Pascual, F.J., Díez Montes, A., Díez Fernández, R., Gómez Barreiro,
 970 J., Dias Da Silva, Í., González Clavijo, E., Ayarza, P., and Alcock, J.E.: The late Variscan
 971 HT/LP metamorphic event in NW and Central Iberia: relationships to crustal thickening,
 972 extension, orocline development and crustal evolution, *Geological Society, London, Special
 973 Publications*, 405(1), 225-247, 2014.
- 974 Martínez Poyatos, D., Nieto, F., Azor, A., and Simancas, J.F.: Relationships between very low-grade
 975 metamorphism and tectonic deformation: Examples from the southern Central Iberian Zone
 976 (Iberian Massif, Variscan Belt), *Journal of the Geological Society*, 158, 953-968, 2001.
- 977 Martínez Poza, A.I., Martínez Poyatos, D., Simancas, J.F., and Azor, A.: La estructura varisca de la
 978 Unidad del Pulo do Lobo (SO del Macizo Ibérico) en las transversales de Aroche y Rosal de
 979 la Frontera (Huelva), *Geogaceta*, 52, 21-24, 2012.
- 980 Massonne, H.J., and Schreyer, W.: Phengite geobarometry based on the limiting assemblage with K-
 981 feldspar, phlogopite, and quartz, *Contributions to Mineralogy and Petrology*, 96, 212-224,
 982 1987.
- 983 Massonne, H.J., and Szpurka, Z.: Thermodynamic properties of white micas on the basis of high-
 984 pressure experiments in the systems K₂O-MgO-Al₂O₃- SiO₂-H₂O and K₂O-FeO-Al₂O₃-
 985 SiO₂-H₂O. *Lithos*, 41, 229-250, 1997.
- 986 Matte, P.: The Variscan collage and orogeny (480-290 Ma) and the tectonic definition of the Armorica
 987 microplate: A review, *Terra Nova*, 13, 122-128, 2001.
- 988 Merriman, R.J., and Frey, M.: Patterns of very low-grade metamorphism in metapelitic rocks, in: *Low-
 989 grade metamorphism*, edited by: Frey, M., and Robinson, D., Blackwell, Oxford, 61-107,
 990 1999.
- 991 Moita, P., Munhá, J., Fonseca, P., Pedro, J., Araújo, A., Tassinari, C., and Palacios, T.: Phase equilibria
 992 and geochronology of Ossa-Morena eclogites, *Actas do XIV Semana de Gequímica / VIII
 993 Congresso de geoquímica dos Países de Língua Portuguesa*, 2, 471-474, 2005.
- 994 Moore, D.M., and Reynolds, R.C. Jr.: *X-ray Diffraction and the Identification and Analysis of Clay
 995 Minerals*, 2nd edition, Oxford University Press, Oxford, 1997.

- 996 Mori, H., Mori, N., Wallis, S., Westaway, R., and Annen, C.: The importance of heating duration for
 997 Raman CM thermometry: evidence from contact metamorphism around the Great Whin Sill
 998 intrusion, UK, *Journal of Metamorphic Geology*, 35(2), 165-180, 2017.
- 999 Munhá, J.: Metamorphic evolution of the south Portuguese/Pulo do Lobo zone, in: *Pre-Mesozoic*
 1000 *Geology of Iberia*, edited by: Dallmeyer, R.D., and Martínez García, E., Springer, Berlin,
 1001 Germany, pp. 363-368, 1990.
- 1002 [Murphy, J. B., Quesada, C., Gutiérrez-Alonso, G., Johnston, S. T. and Weil, A.: Reconciling](#)
 1003 [competing models for the tectono-stratigraphic zonation of the Variscan orogen in Western](#)
 1004 [Europe. *Tectonophysics*, 681, 209-219, 2016.](#)
- 1005 Nieto, F., and Sánchez-Navas, A.: A comparative XRD and TEM study of the physical meaning of
 1006 the white mica «crystallinity» index, *European Journal of Mineralogy*, 6(5), 611-621, 1994.
- 1007 Nieto, F., Mata, M.P., Bauluz, B., Giorgetti, G., Árkai, P., and Peacor, D.R.: Retrograde diagenesis, a
 1008 widespread process on a regional scale, *Clay Minerals*, 40(1), 93-104, 2005.
- 1009 Oliveira, J.T.: Part VI: South Portuguese Zone, stratigraphy and synsedimentary tectonism, in: *Pre-*
 1010 *Mesozoic Geology of Iberia*, edited by: Dallmeyer, R.D., and Martínez García, E., Springer,
 1011 Berlin, Germany, pp. 334-347, 1990
- 1012 Olsson, I.: Regional burial heating vs. local magmatic heat influence of the Röstänga area, Scania,
 1013 southern Sweden, *GFF*, 121(3), 209-214, 1999.
- 1014 Omrani, H., Moazzen, M., Oberhänsli, R., and Moslempour, M.E.: Iranshahr blueschist: subduction
 1015 of the inner Makran oceanic crust, *Journal of Metamorphic Geology*, 35(4), 373-392, 2017.
- 1016 Ordóñez-Casado, B.: Geochronological studies of the Pre-Mesozoic basement of the Iberian Massif:
 1017 the Ossa-Morena Zone and the Allochthonous Complexes within the Central Iberian Zone,
 1018 Ph.D. Thesis, ETH Zurich, 235 pp., 1998.
- 1019 Parra, T., Vidal, O., and Agard, P., A thermodynamic model for Fe-Mg dioctahedral K White micas
 1020 using data from phase-equilibrium experiments and natural pelitic assemblages, *Contrib.*
 1021 *Mineral Petrol.*, 143, 706-732, 2002.
- 1022 Pedro, J., Araujo, A., Fonseca, P., Tassinari, C., and Ribeiro, A.: Geochemistry and U-Pb Zircon Age
 1023 of the Internal Ossa-Morena Zone Ophiolite Sequences: A Remnant of Rheic Ocean in SW
 1024 Iberia, *Oñoliti*, 35(2), 117-130, 2010.
- 1025 Pereira, M.F., Apraiz, A., Chichorro, M., Silva, J.B., and Armstrong, R.A.: Exhumation of high
 1026 pressure rocks in northern Gondwana during the Early Carboniferous (Coimbra-Cordoba
 1027 shear zone, SW Iberian Massif): tectonothermal analysis and U-Th-Pb SHRIMP in-situ
 1028 zircon geochronology, *Gondwana Research*, 17, 440-460, 2010.
- 1029 Pereira, M.F., Chichorro, M., Silva, J.B., Ordóñez-Casado, B., Lee, J.K., and Williams, I.S.: Early
 1030 carboniferous wrenching, exhumation of high-grade metamorphic rocks and basin instability
 1031 in SW Iberia: constraints derived from structural geology and U-Pb and ⁴⁰Ar-³⁹Ar
 1032 geochronology, *Tectonophysics*, 558, 28-44, 2012.
- 1033 Pereira, M.F., Chichorro, M., Williams, I.S., Silva, J.B., Fernández, C., Díaz-Azpiroz, M., Apraiz, A.,
 1034 and Castro, A.: Variscan intra-orogenic extensional tectonics in the Ossa-Morena Zone
 1035 (Évora-Aracena-Lora del Río metamorphic belt, SW Iberian Massif): SHRIMP zircon U-Th-
 1036 Pb geochronology, *Geological Society, London, Special Publications*, 327(1), 215-237, 2009.
- 1037 Pereira, M.F., Martínez Poyatos, D., Pérez-Cáceres, I., Gama, C., and Azor, A.: Comment on
 1038 “Stratigraphy of the Northern Pulo do Lobo Domain, SW Iberia Variscides: A palynological
 1039 contribution” by Pereira, Z. et al. (2018) - *Geobios*, 51, 491-506. *Geobios*, in press, 2019.

- 1040 Pereira, Z., Matos, J., Fernandes, P., and Oliveira, J.T.: Palynostratigraphy and systematic palynology
 1041 of the Devonian and Carboniferous successions of the South Portuguese Zone, Portugal,
 1042 Memórias Geológicas do Instituto Nacional de Engenharia, Tecnologia e Inovação 34,
 1043 Lisboa, 2008.
- 1044 Pereira, Z., Fernandes, P., Matos, J., Jorge, R., and Oliveira, J.T.: Stratigraphy of the Northern Pulo
 1045 do Lobo Domain, SW Iberia Variscides: A palynological contribution, *Geobios*, 51, 491-506,
 1046 2018.
- 1047 Pérez-Cáceres, I., Martínez Poyatos, D., Simancas, J.F., and Azor, A.: The elusive nature of the Rheic
 1048 Ocean in SW Iberia, *Tectonics*, 34, 2429-2450, 2015.
- 1049 Pérez-Cáceres, I., Simancas, J.F., Martínez Poyatos, D., and Azor, A.: Oblique collision and
 1050 deformation partitioning in the SW Iberian Variscides, *Solid Earth*, 7, 857-872, 2016.
- 1051 Pérez-Cáceres, I., Martínez Poyatos, D., Simancas, J.F., and Azor, A.: Testing the Avalonian affinity
 1052 of the South Portuguese Zone and the Neoproterozoic evolution of SW Iberia through
 1053 detrital zircon populations, *Gondwana Research*, 42, 177-192, 2017.
- 1054 [Pérez-Estaún, A., Bea, F. and Vera, J. A.: Macizo Ibérico. Edited by: Vera, J.A., *Geología de España*,
 1055 19-228, 2004.](#)
- 1056 Petschick R.: [http://www.geol-pal.uni-frankfurt.de/
 1057 Staff/Homepages/Petschick/classicsoftware.html# MacDiff](http://www.geol-pal.uni-frankfurt.de/Staff/Homepages/Petschick/classicsoftware.html#MacDiff), 2004.
- 1058 Platt, J. P.: Dynamics of orogenic wedges and the uplift of high-pressure metamorphic rocks,
 1059 *Geological Society of America Bulletin*, 97(9), 1037-1053, 1986.
- 1060 Ponce, C., Simancas, J.F., Azor, A., Martínez Poyatos, D.J., Booth-Rea, G., and Expósito, I.:
 1061 Metamorphism and kinematics of the early deformation in the Variscan suture of SW Iberia,
 1062 *Journal of Metamorphic Geology*, 30(7), 625-638, 2012.
- 1063 Potel, S., Ferreiro-Mählmann, R., Stern, W. B., Mullis, J., and Frey, M.: Very low-grade metamorphic
 1064 evolution of pelitic rocks under high-pressure/low-temperature conditions, NW New
 1065 Caledonia (SW Pacific), *Journal of Petrology*, 47(5), 991-1015, 2006
- 1066 Potel, S., Maison, T., Maillet, M., Sarr, A. C., Doublier, M. P., Trullenque, G., and Mählmann, R. F.:
 1067 Reliability of very low-grade metamorphic methods to decipher basin evolution: Case study
 1068 from the Markstein basin (Southern Vosges, NE France), *Applied Clay Science*, 134, 175-
 1069 185, 2016.
- 1070 Quesada, C.: [Precambrian successions in SW Iberia: their relationship to 'Cadomian' orogenic events.
 1071 Geological Society, London, Special Publications, 51\(1\), 353-362, 1990.](#) Quesada, C.,
 1072 Fonseca, P.E., Munhá, J., Oliveira, J.T., and Ribeiro, A.: The Beja-Acebuches Ophiolite
 1073 (Southern Iberia Variscan fold belt): geological characterization and significance, *Boletín
 1074 Geológico Minero*, 105, 3-49, 1994.
- 1075 [Quesada, C., Braid, J. A., Fernandes, P., Ferreira, P., Jorge, R. S., Matos, J. X., Murphy, J.B., Oliveira,
 1076 J.T., Pedro, J. and Pereira, Z.: SW Iberia Variscan Suture Zone: Oceanic Affinity Units. In
 1077 The Geology of Iberia: A Geodynamic Approach, Volume 2: The Variscan Cycle, edited by:
 1078 Quesada, C., and Oliveira, J.T., Springer. 131-171. Springer, 2019.](#)
- 1079 Ribeiro, A., Munhá, J., Fonseca, P.E., Araujo, A., Pedro, J.C., Mateus, A., Tassinari, C., Machado, G.,
 1080 and Jesus, A.: Variscan ophiolite belts in the Ossa-Morena Zone (Southwest Iberia):
 1081 Geological characterization and geodynamic significance, *Gondwana Research*, 17(2-3), 408-
 1082 421, 2010.

Con formato: Inglés (Reino Unido)

- 1083 Rubio Pascual, F.J., Matas J., and Martín Parra, L.M.: High-pressure metamorphism in the Early
1084 Variscan subduction complex of the SW Iberian Massif, *Tectonophysics*, 592, 187-199, 2013.
- 1085 Sassi, F.P., and Scolari, A.: The b_0 value of the potassic white micas as a barometric indicator in low-
1086 grade metamorphism of pelitic schists, *Contributions to Mineralogy and Petrology*, 45(2),
1087 143-152, 1974.
- 1088 Silva, J. B., Oliveira, J.T., and Ribeiro, A.: South Portuguese Zone, ~~estructural~~ structural outline, in:
1089 Pre-Mesozoic Geology of Iberia, edited by: Dallmeyer, R.D., and Martínez García, E.,
1090 Springer, Berlin, Germany, pp. 348-362, 1990.
- 1091 Simancas, J.F., Carbonell, R., Lodeiro, F.G., Pérez-Estaún, A., Juhlin, C., Ayarza, P., Kashubin, A.,
1092 Azor, A., Martínez Poyatos, D., Almodóvar, G.R., Pascual, E., Sáez, R., and Expósito, I.:
1093 Crustal structure of the transpressional Variscan orogen of SW Iberia: SW Iberia deep
1094 seismic reflection profile (IBERSEIS), *Tectonics*, 22(6), 1062, 2003.
- 1095 Simancas, J.F., Expósito, I., Azor, A., Martínez Poyatos, D., and González Lodeiro, F.: From the
1096 Cadomian orogenesis to the Early Palaeozoic Variscan rifting in Southwest Iberia, *Journal*
1097 *of Iberian Geology*, 30, 53-71, 2004.
- 1098 Simancas, J.F., Carbonell, R., González Lodeiro, F., Pérez-Estaún, A., Juhlin, C., Ayarza, P.,
1099 Kashubin, A., Azor A., Martínez Poyatos, D.J., Sáez, R., Almodóvar, G.R., Pascual R.,
1100 Flecha, I., and Martí, D.: Transpressional collision tectonics and mantle plume dynamics:
1101 The Variscides of southwestern Iberia, *Memoirs, Geol. Soc.*, 32(1), 345-354, 2006.
- 1102 Vázquez, M., Abad, I., Jiménez-Millán, J., Rocha, F.T., Fonseca, P.E., and Chaminé, H.I.: Prograde
1103 epizonal clay mineral assemblages and retrograde alteration in tectonic basins controlled by
1104 major strike-slip zones (W Iberian Variscan chain), *Clay Minerals*, 42(1), 109-128, 2007.
- 1105 Vidal, O., Parra, T., and Trotet, F.: A thermodynamic model for Fe-Mg aluminous chlorite using data
1106 from phase equilibrium experiments and natural pelitic assemblages in the 100-600 °C 1-25
1107 kbar range, *American Journal of Science*, 63, 557-592, 2001.
- 1108 Vidal, O., Parra, T., and Vicillard, P.: Thermodynamic properties of the Tschermak solid solution in
1109 Fe-chlorite: application to natural examples and possible role of oxidation, *American*
1110 *Mineralogist*, 90, 347-358, 2005.
- 1111 Vidal, O., de Andrade, V., Lewin, E., Muñoz, M., Parra, T., and Pascarelli, S.: P-T-deformation-
1112 Fe³⁺/Fe²⁺ mapping at the thin section scale and comparison with XANES mapping.
1113 Application to a garnet-bearing metapelite from the Sambagawa metamorphic belt (Japan),
1114 *Journal of Metamorphic Geology*, 24, 669-683, 2006.
- 1115 Vidal, O., Lanari, P., Munoz, M., Bourdelle, F., and De Andrade, V.: Deciphering temperature,
1116 pressure and oxygen-activity conditions of chlorite formation, *Clay Minerals*, 51(4), 615-633,
1117 2016.
- 1118 Warr, L.N., and Ferreiro Mählmann, R.: Recommendations for Kübler Index standardization, *Clay*
1119 *Minerals*, 50(3), 283-286, 2015.
- 1120 Warr, L.N., and Rice, A.H.N.: Inter-laboratory standardization and calibration of clay mineral
1121 crystallinity and crystallite size data, *Journal of Metamorphic Geology*, 12, 141-152, 1994.
- 1122 Whitney, D.L., and Evans, B.W.: Abbreviations for names of rock-forming minerals, *American*
1123 *mineralogist*, 95(1), 185, 2010.

Figure 1

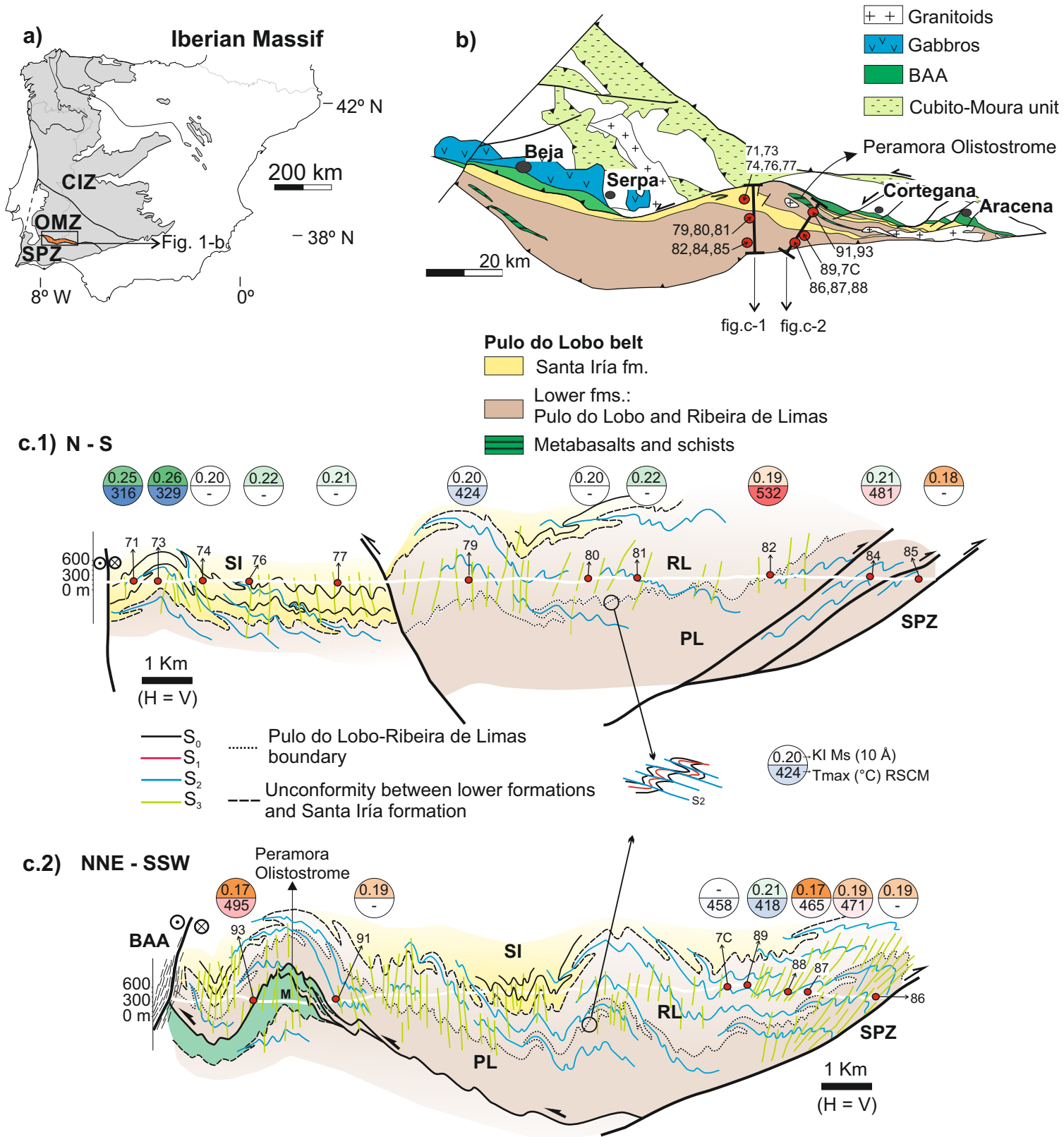


Figure 2

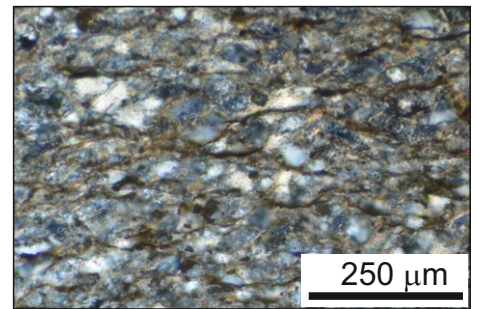
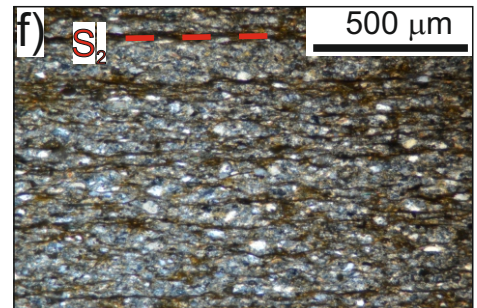
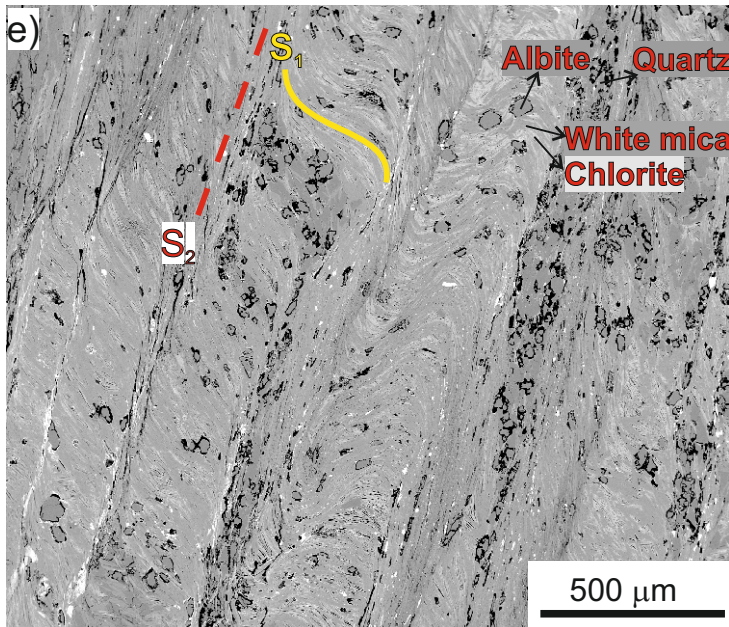
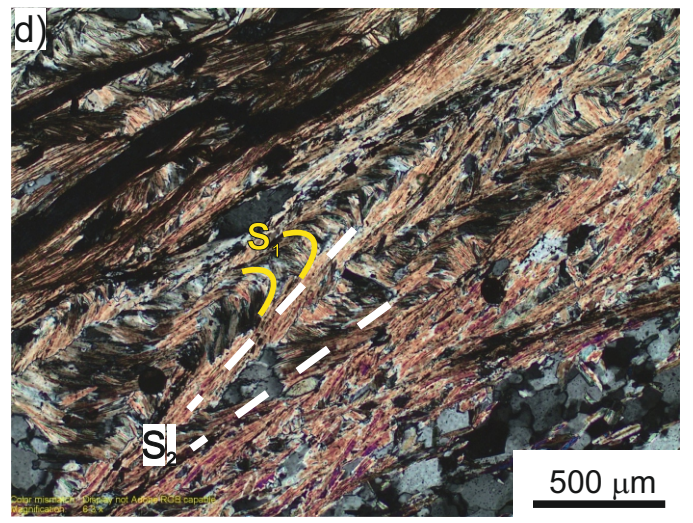
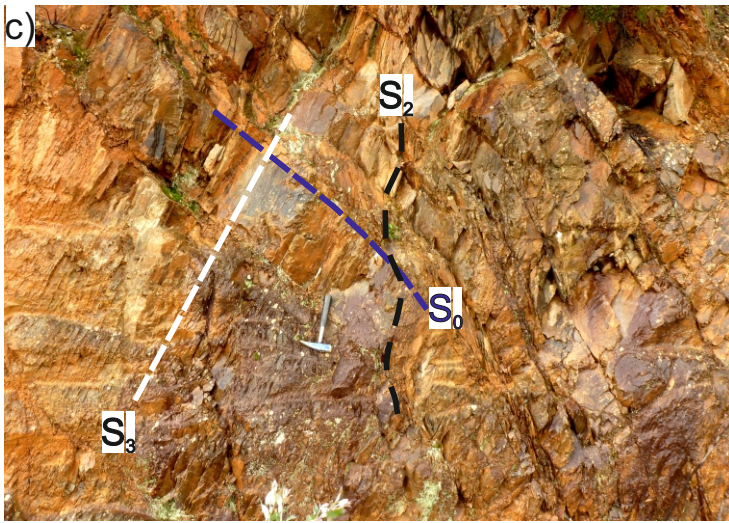
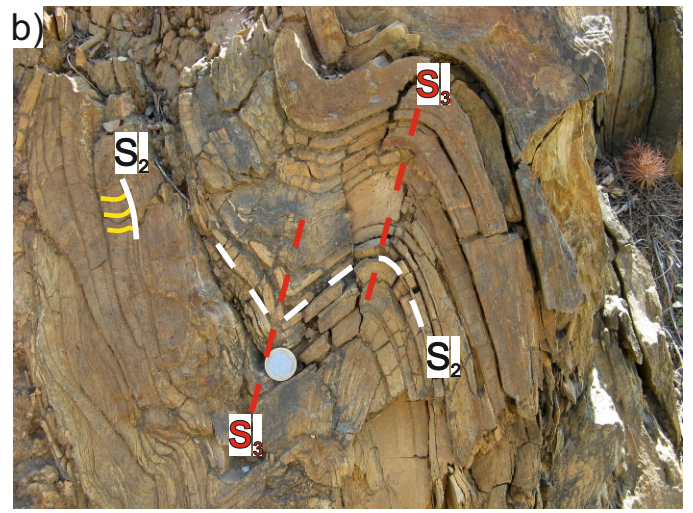
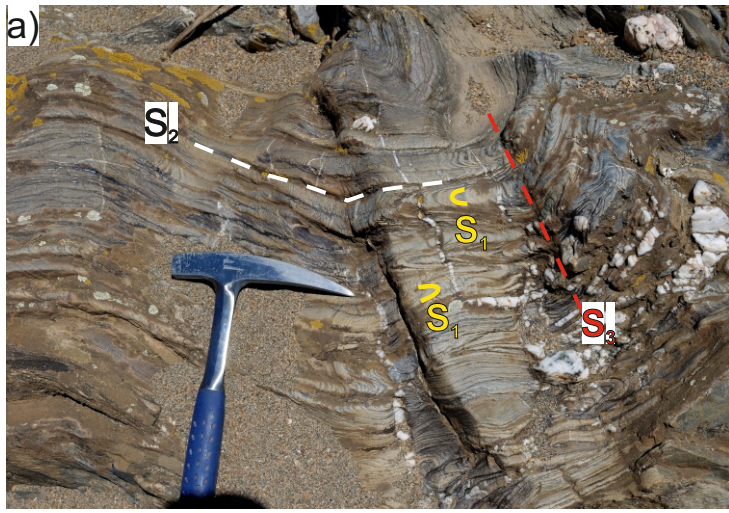


Figure 3

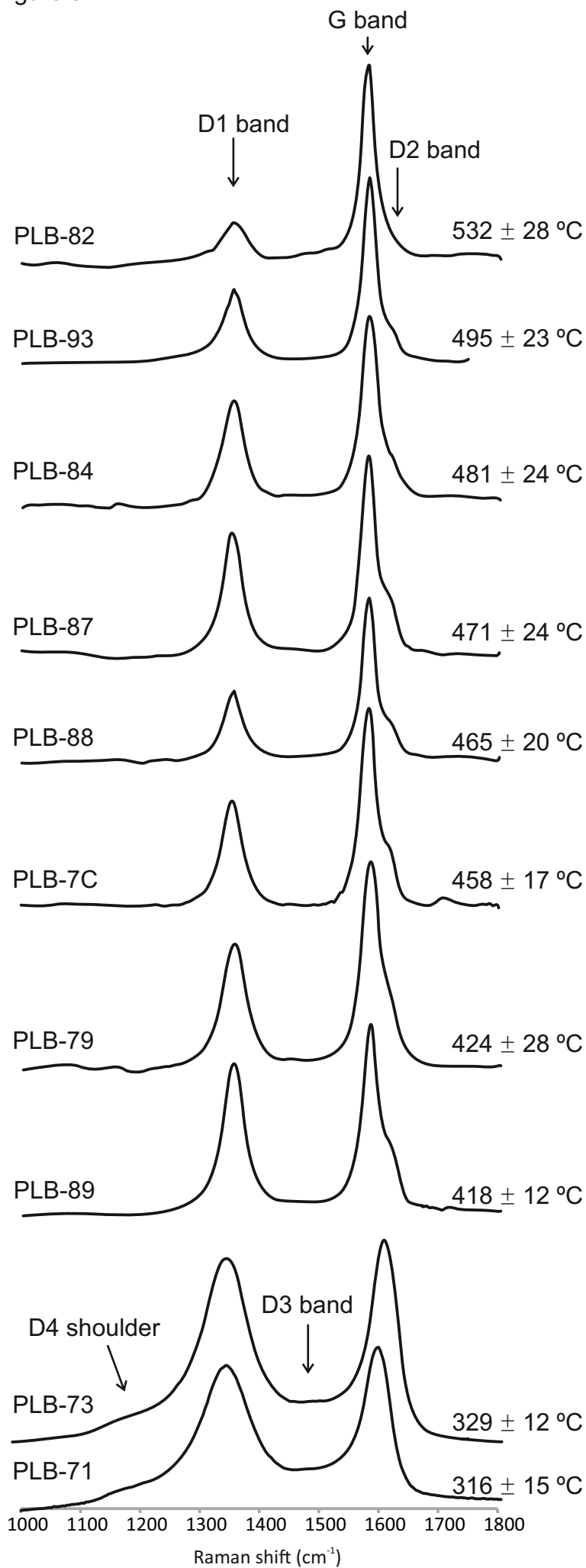


Figure 4

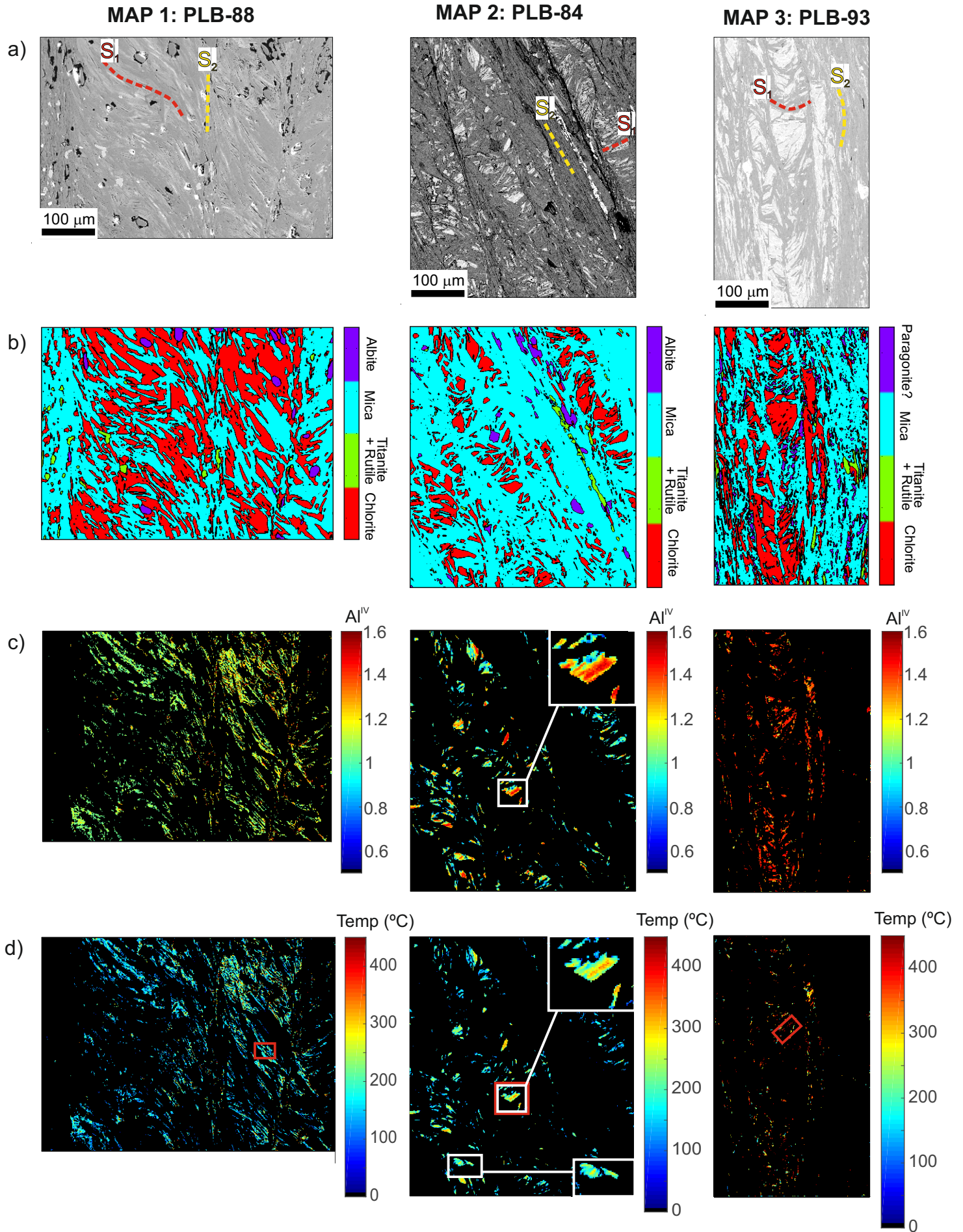


Figure 5

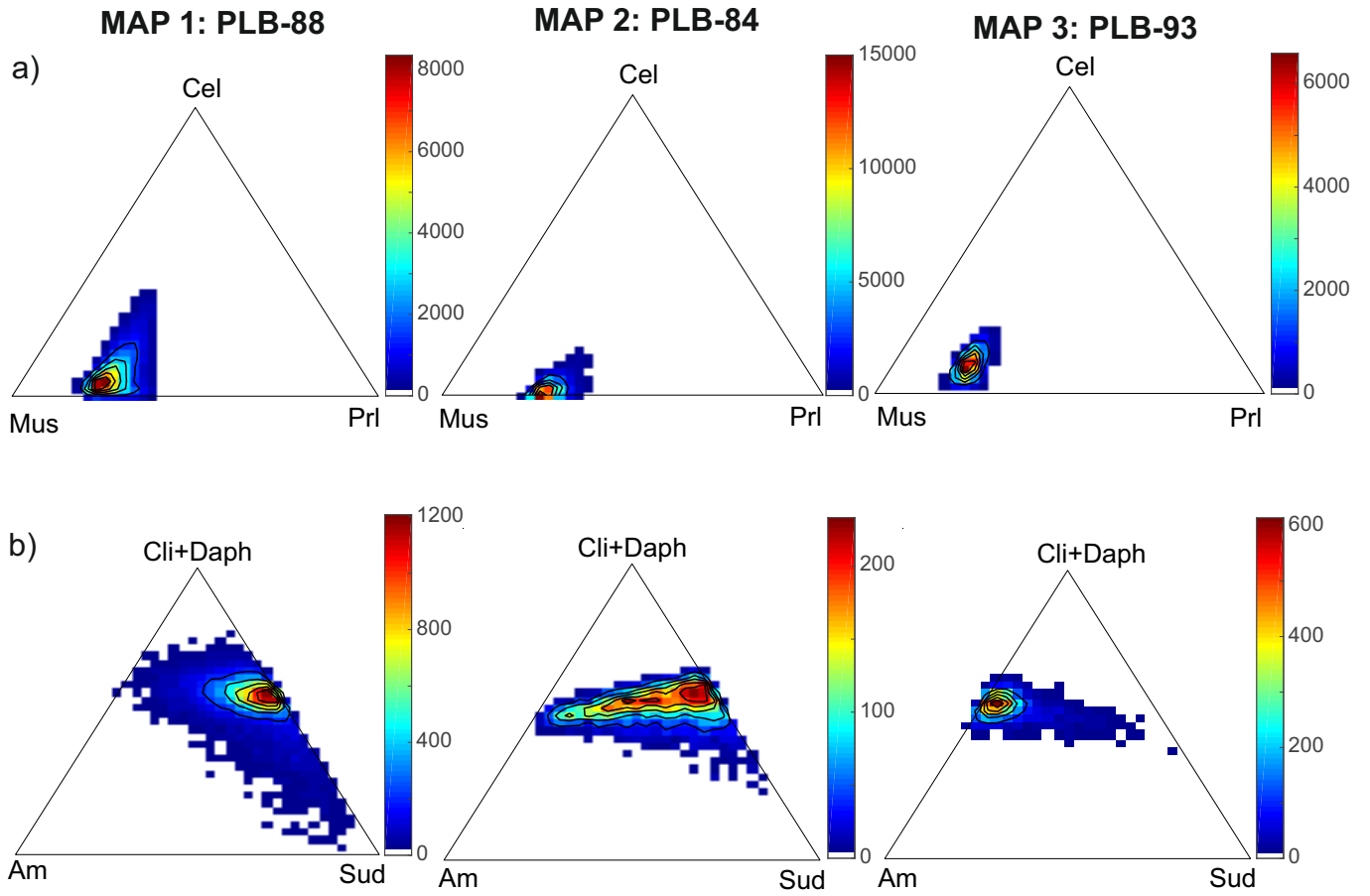


Figure 6

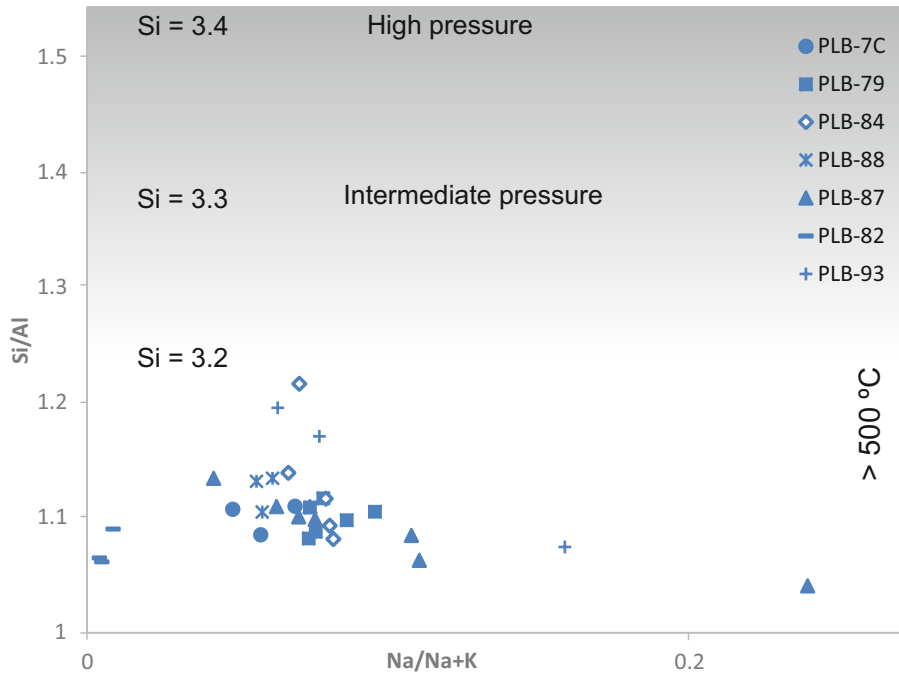
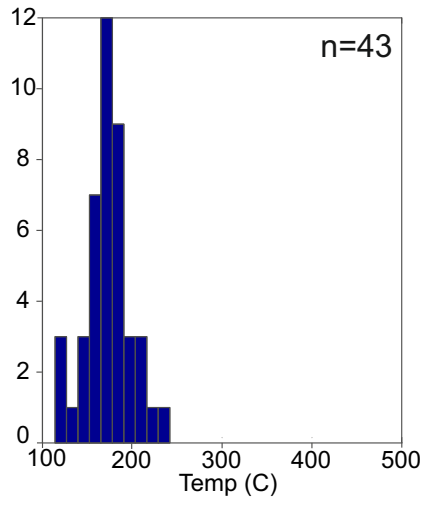
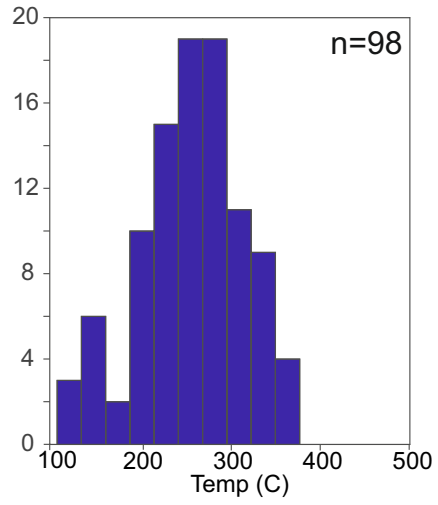


Figure 7

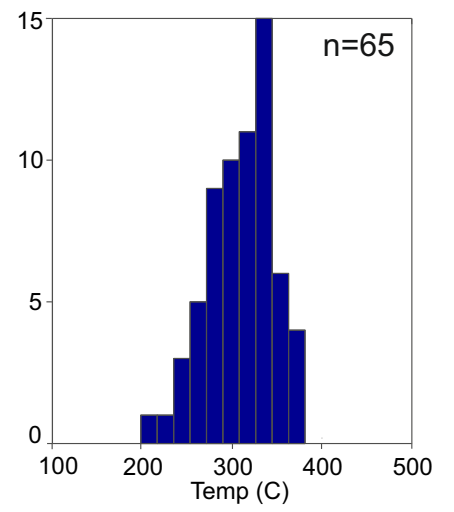
a) MAP 1: PLB-88



MAP 2: PLB-84



MAP 3: PLB-93



b)

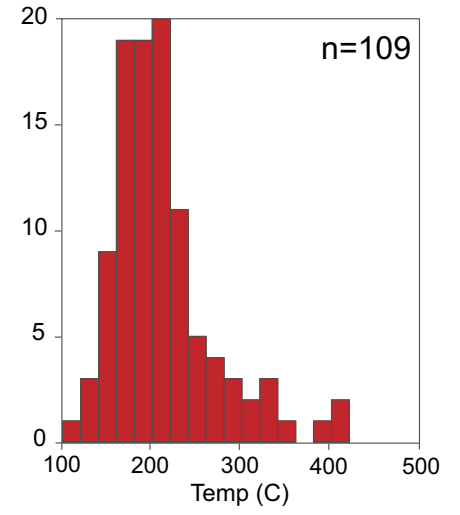
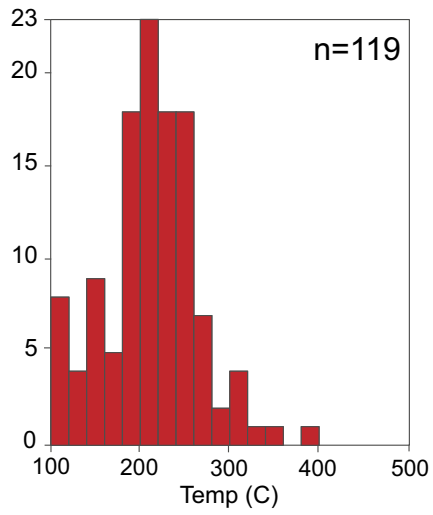
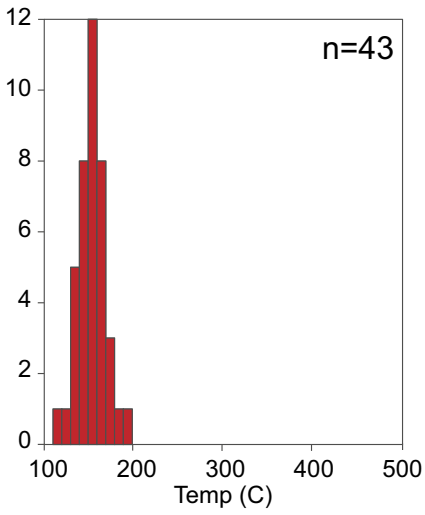


Table 1

Formation	Sample	Mineralogy	FWHM	Basel KI (10 Å)		b (Å)	d ₀₀₁ (Å)	White mica compositions			Chlorite compositions			Chlorite maps	Chlorite thermometry		T _{max} (°C) RSCM	
					<2 μm			% Ms	% Cel	% Prl	% Cli+Daph	% Am	% Sud	(Lanari et al., 2014b)	Vidal et al., 2006	Bourdelle et al., 2013	Mean	Std Dv
	PLB-	Qz + Ms + Fsp+	Å	bulk fraction		Ms	Ms						T (°C)	T (°C)	T (°C)			
Santa Iria (upper formation)	71	Chl	0.221	0.23	0.25	8.991	9.995	-	-	-	-	-	-	-	-	-	316	15
	73	Chl	0.227	0.22	0.26	8.996	9.997	-	-	-	-	-	-	-	-	-	329	12
	74	Chl + C/S	0.164	0.20	0.20	8.999	10.001	-	-	-	-	-	-	-	-	-	-	-
	76	Chl	0.184	0.20	0.22	8.997	9.997	-	-	-	-	-	-	-	-	-	-	-
	77	Chl + C/S	0.171	0.19	0.21	8.998	9.995	-	-	-	-	-	-	-	-	-	-	-
lower fomations	79	Chl + Pg	0.17	0.18	0.20	8.995	9.993	-	-	-	-	-	-	-	-	-	424	28
	80	Chl	0.169	0.18	0.20	9.001	9.988	-	-	-	-	-	-	-	-	-	-	-
	81	Chl + Pg + C/S	0.181	0.19	0.22	-	9.988	-	-	-	-	-	-	-	-	-	-	-
	82	Chl + Pg	0.158	0.17	0.19	8.995	9.986	-	-	-	-	-	-	-	-	-	532	28
	84 (map 2)	Chl + Pg + C/S	0.173	0.17	0.21	8.994	9.988	70-80	0-10	20-30	50	0-50	0-50	150-350	150-375	150-350	481	24
	85	Chl + Pg	0.137	0.17	0.18	8.996	9.996	-	-	-	-	-	-	-	-	-	-	-
	86	Pg + C/S	0.144	0.18	0.19	8.993	9.986	-	-	-	-	-	-	-	-	-	-	-
	87	Chl + Pg	0.144	0.18	0.19	8.998	9.986	-	-	-	-	-	-	-	-	-	471	24
	88 (map 1)	Chl + Pg	0.129	0.18	0.17	8.997	9.990	70-80	0-10	20-30	50	0-10	20-50	100-200	120-230	150-200	465	20
	89	Chl	0.178	0.19	0.21	8.996	9.993	-	-	-	-	-	-	-	-	-	418	12
	91	Chl + Pg	0.143	0.17	0.19	9.000	9.995	-	-	-	-	-	-	-	-	-	-	-
	93 (map 3)	Chl + Pg	0.128	0.18	0.17	9.002	9.990	70-80	0-10	20-30	50	40-50	0-10	200-450	200-380	150-400	495	23
7C	-	-	-	-	-	8.993	-	-	-	-	-	-	-	-	-	-	458	17

Table 2

Time	Deformation/metamorphic phase	Temperature	Low-grade metamorphic conditions
Middle-Upper Carboniferous	S ₃ S ₂ -M ₂	- <300 °C	- Epizone-Anchizone limit
Early Carboniferous (~340 Ma)	Beja-Acebuches and Pulo do Lobo metamafics Thermal imprint		
Upper Devonian	S ₁ -M ₁	~300-450 °C	Epizone